Full-Space Conformal Mapping for the Calculation of the Parameters of Overhead Transmission Lines and Underground Cables

by

Edison Manuel Smith Rodriguez

A Thesis submitted to the Faculty of Graduate Studies of
The University of Manitoba
in partial fulfilment of the requirements of the degree of

MASTER OF SCIENCE

Department of Electrical and Computer Engineering
University of Manitoba
Winnipeg, Canada

Abstract

This thesis presents a method to obtain the per-unit-length electrical parameters of a given overhead transmission line or underground cable in an unbounded space considering the effect of the ground. This is achieved using a two-dimensional conformal mapping technique, which consists of a modified bilinear transformation to map a semi-open half-space problem into a unit circle. The Helmholtz equations describing the quasi-stationary approximation for the electromagnetic field behaviour are solved using finite element method, with the aid of commonly used commercial software program, COMSOL Multiphysics. The per-unit-length resistance, inductance and capacitance are calculated using the proposed mapping method, the truncation of the original space method and then compared with the analytical solution obtained from Carson's approximation for the overhead lines and Wedepohl's formulation for the underground cables.

Acknowledgements

My special gratitude will always be to God who gives and takes away, blessed be His Name.

I also would like to thank my wife for her motivation and support, I will never forget that she left her dreams behind to join me on this adventure.

I would like to thank my parents and brothers for all their love and support throughout my life. And I thank my grandmother for being the strongest person I have ever known and who I now miss the most.

I would like to thank my academic advisors Dr. Behzad Kordi and Dr. Aniruddha Gole for their valuable guidance and encouragement throughout the years this research was conducted.

I would like to thank the examining committee, Dr. Puyan Mojabi and Dr. Masoud Asadzadeh, for reviewing my thesis.

I would like to express my gratitude to the Itaipu Binational and the Itaipu Technological Park for their financial support throughout my studies at the University of Manitoba.

I would like to thank the staff of the Department of Electrical and Computer Engineering, specially Amy Dario for her patience, help and advice.

I could not write this Acknowledgment without thanking Pastors Sunday and Deborah Olukoju and their kids for receiving us and making us feel part of the family.

I would like to thank my friends Juan Cameron, Melinda Altamirano, Eduardo Costa, Andre Jinno, Eduardo Almiron and Maria Jose Patino, who made our stay in Canada even more enjoyable.

Dedication

I dedicate this thesis to my dear wife, Pamela Lafuente Smith, my loving parents, Ali Khalil Yassine and Hilda Rodriguez de Yassine, and my brothers, Rhanda Yassine and Jamal Yassine. I also dedicate it to my beloved grandmother, Sara Kennedy.

Table of Contents

List of Figures

List of Tables

Chapter 1

Introduction

The propagation characteristics of overhead transmission lines and underground cables are intrinsically associated with their longitudinal and transversal electrical parameters, *i.e.*: the frequency-dependent longitudinal impedance and transversal admittance.

It is very important to know the electrical characteristics of power transmission systems for reliable operational conditions of a power system as a whole. The accuracy in the parameter identification is directly related to many issues in power system analysis, such as: fault detection/location in overhead transmission lines and underground cables [4]; correct parameterization of protection systems [5]; appropriate coordination of the insulation [6]; understanding the wave propagation [7]; transient conditions and possible overvoltages in transmission systems, which lead to a correct design of the surge protection [8].

In general, technical literature presents two procedures to identify the electrical parameters of multiconductor transmission lines and cables: by estimation or calculation. The first procedure is based on the current and voltage measurements at both line terminals. Usually, the currents and the voltages, at the sending and the receiving ends of the line, are synchronously obtained using phasor measurement units (PMUs) or fault records obtained from protective relays [9–11]. Therefore, the transmission system can be modeled in the frequency or time domain in order to identify the

parameters: resistance (R), inductance (L), conductance (G) and capacitance (C), based on current and voltage measurements [10]. However, each estimation technique can give a better representation depending on the line geometry, system characteristics and dynamics (transient or steady-state) [9].

The second procedure to obtain the electrical parameters is by calculation based on the geometrical and structural characteristics of the transmission system, such as: height from the ground (or depth for underground cables), conductor characteristics (conductivity, wire shape, cross section, etc), environment in which the conductor is immersed (air, soil, water, etc), distance between conductors (in case of multiconductor transmission lines) [12].

The frequency-dependent impedance of a conductor is composed of two main parts: the impedance due to the skin effect and the earth-return impedance. The first component is given by the non-uniformity of the current distribution over the cross section of the conductor *i.e.*, the current density increases progressively, from the centre toward the surface of the conductor as a function of the frequency of the longitudinal electrical field in the conductor. This phenomenon results in a major concentration of the current through the boundary of the conductor which leads to a non-linear increase of the longitudinal resistance as a function of the frequency. Conventionally, the impedance resulted from the skin effect is calculated by approximations using the Bessel functions and based on the geometrical-physical characteristics of the conductor [13, 14].

The earth-return impedance is calculated from a formulation based on the trigonometric series of Carson [12]. This procedure is carried out taken into account several approximations in the transmission system (overhead line or underground cable) and considering a homogeneous soil, *i.e.*, constant soil conductivity [15]. Despite the above approximations, the analytically-based formulations using Bessel and Carson functions provide accurate results for a wide range of frequencies. However, these formulations present some restrictions to model non-conventional conductor geometries (*e.g.* sector-shaped cables), non-homogeneous soil configurations or complex cases where the conductor is on the surface of the ground [16].

The well-established finite element method (FEM) is a solution to overcome the problem

with non-conventional geometries in the cross section of multiconductor cables and arbitrary non-homogeneous problems. Besides, FEM presents several advantages over integration methods for solution of electromagnetic problems taking into account a non-homogeneous media and non-linear situations [17]. Nevertheless, the FEM requires suitable techniques to deal with unbounded problems. Despite the notable increase of the computational resources in the last decades (computational memory and processing), finite element open boundary techniques are necessary. Theoretically, an infinite domain requires a very large amount of computational memory which consequently requires an outer truncation boundary to overcome this problem.

In the electrostatic case, the electrostatic field can be neglected (considered as zero) at a point far away from the region of interest. The resolution of unbounded problems is not straight-forward, because in the magnetostatic or quasi-static cases, unlike the electrostatic case, the electric scalar potential cannot be neglected [18]. Based on this statement, it is then necessary to represent an infinite domain using a finite element open boundary technique, making the outer boundary to best represent the exterior region. Thus, for static and dynamic fields, the outer boundary modeling should not present waves reflections, *i.e.*, the boundary between the internal and the external regions are represented as an impedance junction without wave reflection. A number of techniques have been proposed in the past two decades for the simulation of electromagnetic fields at the outer boundary with the implicit or explicit modeling of the impedance junction [17].

Chen and Konrad describe an extensive review on the principal methods applied for representation of the open boundary in FEM [17]. Among the several well-established techniques discussed in this reference, some of them are worth mentioning to show how the techniques have evolved, emphasizing their principal advantages and restrictions:

- Truncation of outer boundaries [19, 20]
- Iterative solutions [21]
- Ballooning [22–24]

- Infinite elements [25–28]
- Spatial transformations [29–31]

The first open boundary technique, truncation of outer boundaries, consists in the hypothesis that the potential and its derivative are null for a very distant outer boundary, which is a simple and intuitive approach. This technique is accurate for a very far away outer boundary which results in a huge allocation of computational memory and a significant processing effort. The truncation of an outer boundary following a general rule in which the distance of the centre of the object to be studied to the outer boundary should be at least five times the distance of the centre of the object to its more external surface, *e.g.*: the radius of the transversal section of a single-conductor cable [17, 19, 20].

The open boundary technique by iterative solutions is a complementary criteria for the truncation of the outer boundary. In order to improve the accuracy of the truncation of the limited inner boundary, an iterative procedure to shift the outer boundary was developed [17]. This method varies the outer boundary as a function of the field strength. The technique by iterative solutions consists of shifting the outer boundary up to a determined value of the field potential, which means that the outer boundary is defined based on the value of the field strength at a determined point with a variable distance from the object of study [21]. However, usually this technique does not imply in reduction of the computational memory allocation and processing, if compared to the conventional truncation of the outer boundary, because several matrix inversions and recursive mesh generations are required for the iterative solutions [17].

The ballooning technique represents an improvement over the outer boundary truncation method [17]. This technique consists of the representation of a surrounding area, around a solution centre, characterized by a finite element mesh. In this approach, the external area of the solution centre is surrounded by an annular area composed of several annular nodes. The referred annular nodes, surrounding the solution centre (*e.g.* the transversal section of a conductor cable), have similar geometry and compose the inner and outer boundaries. The outer boundary is recur-

sively extended from the solution centre following the same geometry of the annular nodes, *i.e.*, a fixed geometric progression denominated as mapping ratio in the technical literature [17, 22, 23]. Thus, the mapping ratio is characterized by the increment of new annulus surrounding the previous one which is represented by the same geometry but with a smaller cross section. The transversal section of the outer boundary increases in a geometric progression which leads the system to a fast convergence to an error close to zero [23]. Despite these improvements this technique requires some criteria to select the centre point and a careful geometric progression setting for the mapping ratio. Furthermore, it may become difficult to apply the required symmetry conditions and get the solutions in the exterior region. It is also important to take into account that the Ballooning technique is restricted to Laplacian operators and convex geometries [17].

A well-established technique to deal with truncation of the open boundary in FEM is by infinite elements. There are two main variations of this technique available in the technical literature: decay interpolation functions and mapped finite elements [25,27,28]. The first technique consists basically of the field decay as a function of the radial distance from the centre point, which is calculated by a decay interpolation function, as explicitly suggested in the technique [17]. The decay function in the external region is set according to the application, since the asymptotic field varies also depending of the problem to be solved. The solution by decay interpolation functions assumes that the field is null at the boundary of the region to be analyzed [26]. On the other hand, in mapped finite element, the domain represented by finite elements is transformed into an infinite domain. The proposed transformation is carried out considering a singular mapping function [25]. The mapping function is applied only for the Jacobian transformation since the variable field are in fact represented by the finite element interpolation functions [17].

The spatial transformations technique has an inverse procedure compared to the method using infinite elements. The infinite elements use mapping interpolation functions to convert a finite domain to an infinite domain, while the spatial transformation converts a physical unbounded domain into a finite domain by conformal or other geometrical mapping procedures [17]. A detailed

description on the conformal mapping approach is employed in this dissertation, since this technique will be applied to identify the longitudinal parameters of cables. Conformal Mapping has been used in several research studies, such as: calculation of two-dimensional bounded scalar field problems using complex analytic functions, also known as mapping functions [29]; calculation of axi-symmetric open boundary problems [30]; solution of waveguide problems [31].

1.1 Thesis Outline

This thesis is composed of six chapters including this introductory chapter.

In Chapter 2, the main analytical equations for the calculation of the electric parameters of overhead transmission lines and underground cables are derived.

In Chapter 3, all the background theories behind the proposed method in this thesis are presented. This includes: the governing equations of the electromagnetic fields; the finite element method, which is the numerical method employed for solving partial differential equations; and the conformal mapping which is the transformation scheme used to alleviate truncation problems.

The method proposed in Chapter 4 basically consists in transforming an unbounded space into two unit circles, the upper one representing the air domain and the lower one representing the ground domain. The resistive losses, magnetic energies and electric energies resulting from the overhead line or underground cable under study are calculated in the mapped domain and then used to determine the per-unit-length resistances, inductances and capacitances, respectively.

In Chapter 5, the results of several case studies are presented using the proposed method and then compared with the analytical formulations. The sector-shaped cable is also studied, but unlike the other cases, there is no analytical solution available.

In Chapter 6, the conclusions of this thesis and the recommendations for future research are presented.

1.2 Contributions

It is important to note that this thesis is the continuation of the work of [16], with the addition of the calculation of the transverse admittance and some overhead transmission line with typical structural and geometrical configurations. The main contributions of this thesis are summarized below:

- It is shown how to use a conformal spatial transformation to transform an unbounded domain into a bounded space, which alleviates truncation problems.
- This mapping technique together with the finite element method is then used for the determination of the per-unit-length parameter of some cases of overhead transmission lines and underground cables.
- Furthermore, it it is shown that this method is able to obtain the correct results for some trivial cases which count with analytical solution to prove that this method can also be applied to non-traditional geometries, specially in those cases where there are no analytical solution.

Chapter 2

Analytical Calculation of the Electric Parameters of Transmission Lines

It is known that in the study of the transmission lines' performance, the transmission of electricity is directly influenced by the values of its electric parameters and the geometry of the conductors. The calculation of the parameters within an acceptable accuracy is necessary to obtain reliable data in the design of transmission lines [32]. There are four main parameters for modeling general lines: longitudinal resistance and inductance, transverse capacitance and conductance. In this chapter, a detailed description is given of how the parameters of a multiconductor transmission line are calculated, considering their distributed nature. Technical information and equations in general are obtained from [1] and [2].

2.1 Overhead Transmission Lines

2.1.1 Longitudinal Impedance of the Line

The self and mutual impedances in the transmission line equations, in the frequency domain, can be obtained from the solution of the Maxwell's equations taking into account the boundary

conditions of the conductor itself, the air and the ground. Since these three materials can be characterized by conductivity, magnetic permeability, and dielectric permittivity, it can be shown that the impedances of the line may be described in terms of the physical properties of the system (conductors, air and ground) and the frequency [12].

For the purpose of calculation, the longitudinal impedance of a transmission line is divided into three components: external impedance (Z_{ext}); internal impedance (Z_{int}); and impedance due to current returning through ground (Z_g). The total longitudinal impedance of the line corresponds to the sum of these three components [33]:

$$Z(\omega) = Z_{ext}(\omega) + Z_{int}(\omega) + Z_g(\omega) \tag{2.1}$$

External Impedance

The external impedance results from the action of the magnetic field in the air, considering that the conductor and the line are ideal. Fig. 2.1 represents the conductors i and k of a generic two-phase transmission line over an ideal ground [12]. The radius of the conductors i and k are r_i and r_k, respectively. The fictitious conductors i' and k' are images of conductors i and k, respectively. The magnetic permeability of air μ_0 is $4\pi 10^{-7}$ [H/m].

The self and mutual (external) impedances, for conductors i and k, are given by [2]:

$$z_{ext_{ik}}(\omega) = z_{ext_{ki}}(\omega) = j\omega\frac{\mu_0}{2\pi}\ln\left(\frac{D_{ik}}{d_{ik}}\right) \tag{2.2a}$$

$$z_{ext_{ii}}(\omega) = j\omega\frac{\mu_0}{2\pi}\ln\left(\frac{2h_i}{r_i}\right) \tag{2.2b}$$

$$z_{ext_{kk}}(\omega) = j\omega\frac{\mu_0}{2\pi}\ln\left(\frac{2h_k}{r_k}\right) \tag{2.2c}$$

$z_{ext_{ik}}$ and $z_{ext_{ki}}$ are the mutual (external) impedances between both conductors, $z_{ext_{ii}}$ is the self (external) impedance with respect to conductor i and $z_{ext_{kk}}$ is the self (external) impedance

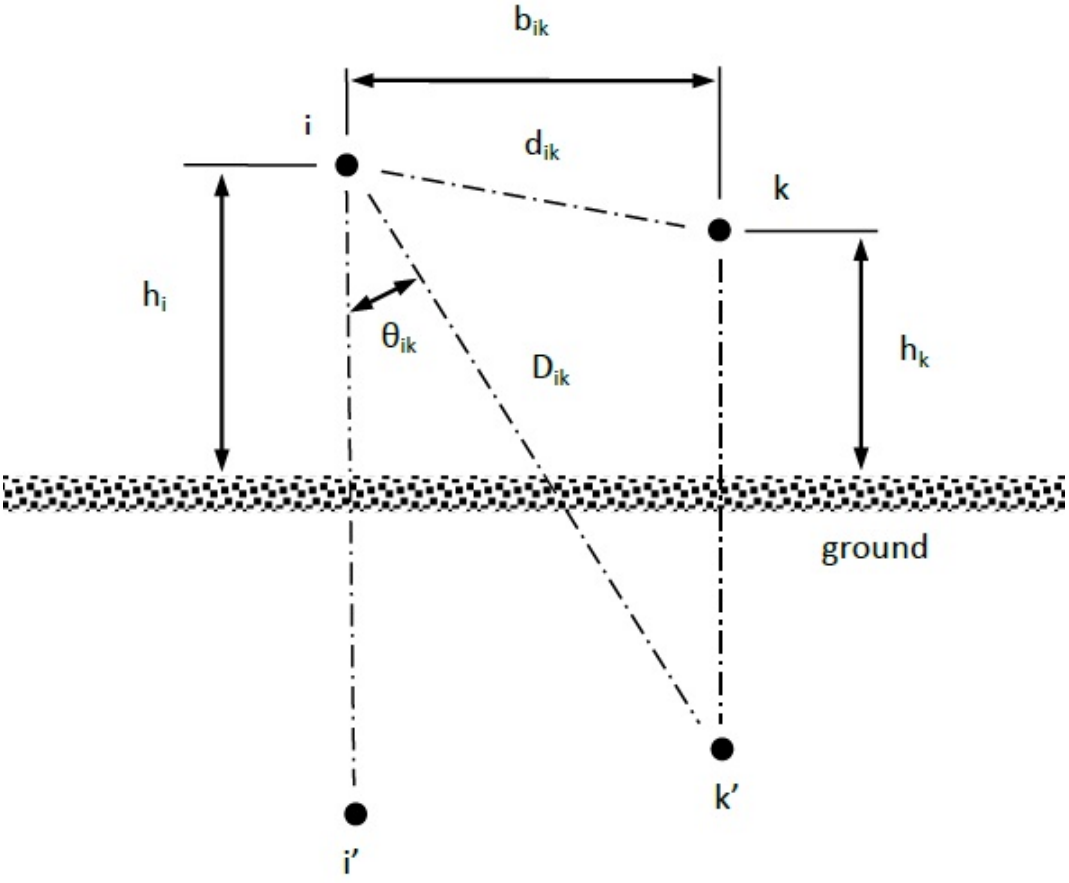

Fig. 2.1: Conductors i and k and their respective images i' and k'.

with respect to conductor k, all in [Ω/m]. ω is the angular velocity related to frequency f given by:

$$\omega = 2\pi f \tag{2.3}$$

The external impedance, as seen in the above equations, represents an inductive reactance. Therefore, the external impedance can be described as:

$$z_{ext}(\omega) = j\omega l_{ext} \tag{2.4}$$

The external inductances can be defined by the following expressions [2]:

$$l_{ext_{ik}} = l_{ext_{ki}} = \frac{\mu_0}{2\pi} \ln\left(\frac{D_{ik}}{d_{ik}}\right) \tag{2.5a}$$

$$l_{ext_{ii}} = \frac{\mu_0}{2\pi} \ln\left(\frac{2h_i}{r_i}\right) \tag{2.5b}$$

$$l_{ext_{kk}} = \frac{\mu_0}{2\pi} \ln\left(\frac{2h_k}{r_k}\right) \tag{2.5c}$$

$l_{ext_{ik}}$ and $l_{ext_{ki}}$ are the mutual (external) inductances between both conductors, $l_{ext_{ii}}$ and $l_{ext_{kk}}$) are the self (external) impedances with respect to conductor i and k, respectively. The external inductances are given in [H/m].

Observing the equations described in this section, it can be stated that they are exclusively dependent on the geometry of the line, the physical characteristics of the conductors and the medium in which the line is inserted.

Thus, for a generic line with n phases whereas each phase consists of one conductor, the external impedance matrix can be written as:

$$\begin{aligned}[Z_{ext}(\omega)] &= j\omega\frac{\mu_0}{2\pi}\begin{bmatrix} \ln\left(\frac{2h_1}{r_1}\right) & \ln\left(\frac{D_{12}}{d_{12}}\right) & \cdots & \ln\left(\frac{D_{1n}}{d_{1n}}\right) \\ \ln\left(\frac{D_{21}}{d_{21}}\right) & \ln\left(\frac{2h_2}{r_2}\right) & \cdots & \ln\left(\frac{D_{2n}}{d_{2n}}\right) \\ \vdots & \vdots & \ddots & \vdots \\ \ln\left(\frac{D_{n1}}{d_{n1}}\right) & \ln\left(\frac{D_{n2}}{d_{n2}}\right) & \cdots & \ln\left(\frac{2h_n}{r_n}\right) \end{bmatrix} \\ &= \begin{bmatrix} z_{ext_{11}} & z_{ext_{12}} & \cdots & z_{ext_{1n}} \\ z_{ext_{21}} & z_{ext_{22}} & \cdots & z_{ext_{2n}} \\ \vdots & \vdots & \ddots & \vdots \\ z_{ext_{n1}} & z_{ext_{n2}} & \cdots & z_{ext_{nn}} \end{bmatrix} \end{aligned} \tag{2.6}$$

Equation (2.6) can be written in a compact form as:

$$[Z_{ext}(\omega)] = j\omega[L_{ext}] \tag{2.7}$$

The external inductance matrix, for n phases, can be written generically as:

$$[L_{ext}] = \frac{\mu_0}{2\pi}\begin{bmatrix} \ln\left(\frac{2h_1}{r_1}\right) & \ln\left(\frac{D_{12}}{d_{12}}\right) & \cdots & \ln\left(\frac{D_{1n}}{d_{1n}}\right) \\ \ln\left(\frac{D_{21}}{d_{21}}\right) & \ln\left(\frac{2h_2}{r_2}\right) & \cdots & \ln\left(\frac{D_{2n}}{d_{2n}}\right) \\ \vdots & \vdots & \ddots & \vdots \\ \ln\left(\frac{D_{n1}}{d_{n1}}\right) & \ln\left(\frac{D_{n2}}{d_{n2}}\right) & \cdots & \ln\left(\frac{2h_n}{r_n}\right) \end{bmatrix} \tag{2.8}$$

It is observed that the matrix $[L_{ext}]$ is a function of the geometry of the conductors and the physical characteristics of the medium, being independent of frequency variation.

Internal Impedance Due To Skin Effect

The uniform distribution of the current over the cross section of a conductor is observed only in DC systems. For AC systems, the current distribution becomes non-uniform. The current density increases progressively, from the centre toward the surface of the conductor, in proportion to the increase in frequency. This phenomenon is called skin effect [1].

Fig. 2.2 describes the skin effect on a conductor based on the geometry and on the current density across the cross section [1].

Considering different longitudinal filaments perpendicular to the cross section of the conductor in Fig. 2.2, those located on the surface are not linked to the internal flux. The flux linkage in a filament near the surface is lower than the flux linkage in an innermost filament. The non-uniformity of the flux linkage is the cause of the skin effect.

The current density and, subsequently, the portion of the impedance due to the skin effect in

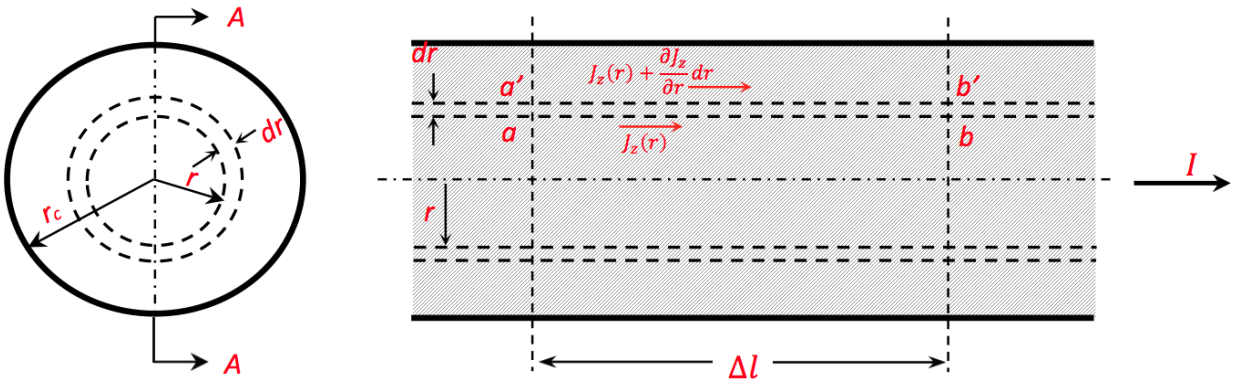

Fig. 2.2: Cross and longitudinal sections of a cylindrical conductor [1].

the conductor can be obtained from a special form of the Bessel differential equation [34]:

$$\frac{d^2y}{dx^2} + \frac{1}{x}\frac{dy}{dx} + \left(k^2 - \frac{n^2}{x^2}\right) y = 0 \tag{2.9}$$

The Bessel equation of order zero ($n = 0$) is given by:

$$\frac{d^2y}{dx^2} + \frac{1}{x}\frac{dy}{dx} + k^2 y = 0 \tag{2.10}$$

The solutions of Equation (2.10) are called Bessel functions of order zero. Because of the assumed symmetry, the current density is z directed and independent of length and angle but it is a function of radius r, so that the Bessel equation applied to the current density is [2]:

$$\frac{d^2J_z(r)}{dr^2} + \frac{1}{r}\frac{dJ_z(r)}{dr} + k^2 J_z(r) = 0 \tag{2.11}$$

where

$$k^2 = -j\omega\mu\sigma \tag{2.12}$$

In Equation (2.11), $J_z(r)$, or J_z from now on, is a complex function which represents the current

density as a function of radial distance from the centre of the conductor. In Equation (2.12), σ and μ are the conductivity and magnetic permeability of the conductor, respectively.

The solution of Equation (2.11) is be given by:

$$J_z = a_0 \sum_{i=0}^{\infty} \left(\frac{j\omega\mu\sigma}{4} \right)^i \frac{r^{2i}}{(i!)^2} \tag{2.13}$$

By separating the real and imaginary part of Equation (2.13) results in:

$$J_z = a_0 \left[ber\left(\frac{\sqrt{2}}{\delta} r \right) + jbei\left(\frac{\sqrt{2}}{\delta} r \right) \right] \tag{2.14}$$

where

$$ber\left(\frac{\sqrt{2}}{\delta} r \right) = 1 - \frac{\left(\frac{\sqrt{2}}{\delta} r \right)^4}{4^2(2!)^2} + \frac{\left(\frac{\sqrt{2}}{\delta} r \right)^8}{4^4(4!)^2} + \cdots \tag{2.15a}$$

$$bei\left(\frac{\sqrt{2}}{\delta} r \right) = \frac{\left(\frac{\sqrt{2}}{\delta} r \right)^2}{4(1!)^2} - \frac{\left(\frac{\sqrt{2}}{\delta} r \right)^6}{4^3(3!)^2} + \frac{\left(\frac{\sqrt{2}}{\delta} r \right)^{10}}{4^5(5!)^2} + \cdots \tag{2.15b}$$

and δ is known as the skin depth or penetration depth, and it is given by:

$$\delta = \frac{1}{\sqrt{\pi f \mu \sigma}} \tag{2.16}$$

The terms *ber* and *bei* are the real and imaginary parts, respectively, of the Bessel function of the first kind [2].

The coefficient a_0 can be determined if the current density on the surface of the conductor $J_z(r = r_w)$ is known:

$$J_z(r_w) = a_0 \left[ber\left(\frac{\sqrt{2}}{\delta} r_w \right) + jbei\left(\frac{\sqrt{2}}{\delta} r_w \right) \right] \tag{2.17}$$

Isolating a_0 in Equation (2.17) and substituting in Equation (2.14) yields:

$$J_z = J_z(r_w)\frac{ber\left(\frac{\sqrt{2}}{\delta}r\right) + jbei\left(\frac{\sqrt{2}}{\delta}r\right)}{ber\left(\frac{\sqrt{2}}{\delta}r_w\right) + jbei\left(\frac{\sqrt{2}}{\delta}r_w\right)} \tag{2.18}$$

Equation (2.18) gives the current density at any point in the conductor as a function of the current density on the surface.

To determine the internal impedance of a conductor where the current is not distributed uniformly over its cross section, it is necessary to know the current density in a cylindrical conductor as given by Equation (2.18). The internal impedance is given only by the resistance of the conductor and the internal flux linkage.

The total current in the conductor can be determined by Ampere's law around the conductor surface (taking into consideration that the displacement current within the conductor is much less than the conduction current) [2]:

$$\begin{aligned} I &= \oint H \cdot dl \\ &= 2\pi r H_\phi|_{r=r_w} \end{aligned} \tag{2.19}$$

The magnetic field can be obtained from Faraday's law ($\nabla \times \mathbf{E} = -j\omega\mathbf{B}$) multiplied by the conductor conductivity and considering the relation of the current density and the electric field ($\mathbf{J} = \sigma\mathbf{E}$) and the relation of the magnetic fields ($\mathbf{B} = \mu\mathbf{H}$), which yields:

$$\nabla \times \mathbf{J} = -j\omega\mu\sigma\mathbf{H} \tag{2.20}$$

Recalling that the current density is z directed and it depends only on r, and that the magnetic field is ϕ directed, Equation (2.20) simplifies to:

$$\frac{dJ_z}{dr} = j\omega\mu\sigma H_\phi \tag{2.21}$$

Isolating H_ϕ in Equation (2.21), and calculating the derivative of Equation (2.18) with respect to r, and substituting these into Equation (2.19) gives the total current in terms of the current at the conductor surface. The mathematical formulation of the per-unit-length internal impedance of the conductor as a function of frequency is obtained dividing the longitudinal electric field at the surface of the conductor by the current flowing inside the conductor [35], thereby, the internal impedance becomes:

$$\begin{aligned} z_{int}(\omega) &= \frac{E_z|_{r=r_w}}{I} = \frac{j\omega\mu\sigma}{2\pi r_w\sigma}\frac{J_z|_{r=r_w}}{\frac{dJ_z}{dr}|_{r=r_w}} \\ &= \frac{1}{\sqrt{2}\pi r_w\sigma\delta}\left[\frac{ber(q)+jbei(q)}{bei'(q)-jber'(q)}\right] \end{aligned} \tag{2.22}$$

where

$$ber'(q) = \frac{d}{dq}ber(q) \tag{2.23a}$$

$$bei'(q) = \frac{d}{dq}bei(q) \tag{2.23b}$$

and

$$q = \sqrt{2}\frac{r_w}{\delta} \tag{2.24}$$

Therefore, the internal impedance of a conductor can be determined at any frequency provided that the radius, the conductivity and the permeability are known. To be consistent with the International System of Units (SI), the conductivity is given in [S/m] [1].

The total internal impedance consists of a resistance (r) and an inductive reactance ($j\omega l_i$):

$$z_{int}(\omega) = r + j\omega l_i \tag{2.25}$$

Separating the real and imaginary parts of Equation (2.22) gives the conductor's resistance

and internal inductance [2]:

$$\frac{r}{r_{dc}} = \frac{q}{2}\left[\frac{ber(q)bei'(q) - bei(q)ber'(q)}{(ber'(q))^2 + (bei'(q))^2}\right] \tag{2.26a}$$

$$\frac{l_i}{l_{i_{dc}}} = \frac{4}{q}\left[\frac{bei(q)bei'(q) - ber(q)ber'(q)}{(ber'(q))^2 + (bei'(q))^2}\right] \tag{2.26b}$$

where

$$r_{dc} = \frac{1}{\sigma\pi r_w^2} \tag{2.27a}$$

$$l_{i_{dc}} = \frac{\mu_0}{8\pi} = 0.5 \times 10^{-7} \tag{2.27b}$$

are, respectively, the dc per-unit-length resistance [Ω/m] and internal inductance [H/m] of the conductor.

Thus, for a generic line with n phases where each phase consists of one conductor, the internal impedance matrix can be written as:

$$[Z_{int}(\omega)] = \begin{bmatrix} z_{int_{11}} & 0 & \cdots & 0 \\ 0 & z_{int_{22}} & \cdots & 0 \\ \vdots & \vdots & \ddots & \vdots \\ 0 & 0 & \cdots & z_{int_{nn}} \end{bmatrix} \tag{2.28}$$

Equation (2.28) can be written in a compact form as:

$$[Z_{int}(\omega)] = [R_{int}] + j\omega[L_{int}] \tag{2.29}$$

The internal resistance and inductance matrices, for n phases, can be written generically as:

$$[R_{int}(\omega)] = \begin{bmatrix} r_{int_{11}} & 0 & \cdots & 0 \\ 0 & r_{int_{22}} & \cdots & 0 \\ \vdots & \vdots & \ddots & \vdots \\ 0 & 0 & \cdots & r_{int_{nn}} \end{bmatrix} \tag{2.30a}$$

$$[L_{int}(\omega)] = \begin{bmatrix} l_{int_{11}} & 0 & \cdots & 0 \\ 0 & l_{int_{22}} & \cdots & 0 \\ \vdots & \vdots & \ddots & \vdots \\ 0 & 0 & \cdots & l_{int_{nn}} \end{bmatrix} \tag{2.30b}$$

It is observed that the matrices $[R_{int}]$ and $[L_{int}]$ are diagonal matrices, *i.e.*, they have no mutual components, and they are frequency-dependent due to skin effect, as described before.

Ground Impedance

Since the ground is not an ideal conductor, *i.e.*, it has finite conductivity, it can be observed that the existence of displacement and conduction currents in the (lossy) ground affect the resultant magnetic flux. This phenomenon is known as ground effect. Given this information, the ground impedance can be written in two portions: considering the ideal ground and another one considering the currents flowing in the ground.

The ground effect increases the resistance and inductance of the total longitudinal impedance. The ground resistance becomes dominant in the total line resistance for higher frequencies [36].

In practice, contrary to what happens in a perfect ground conductor, the returning currents do not flow only at the surface. For this reason, it is not reasonable to replace the ground returning currents effect by an ideal image conductor as shown in Fig. 2.1. Therefore, disregarding this effect, especially in electromagnetic transients studies (high frequencies), produces inaccurate results, which are not consistent with reality. Thus, studying the propagation of electromagnetic waves in

a line above a lossy ground becomes more complicated [37].

The calculation of the ground impedance, for overhead transmission lines over lossy ground, was derived satisfactorily for the first time in 1926 by Carson in [7] and Pollaczek in [38]. These papers were written independently, and since Pollaczek's equations are more generic, they can be applied for underground cables as well [39].

Carson considered conductors parallel to the ground, assuming a uniform resistivity and infinite length. The self and mutual (ground) impedances, respectively, are given by [15]:

$$z_{g_{ii}}^{Carson}(\omega) = \frac{j\omega\mu_0}{\pi} \int_0^\infty \frac{e^{-2h_i u}}{\sqrt{u^2 + j\omega\mu_0\sigma_g} + u}\, \mathrm{d}u \tag{2.31a}$$

$$z_{g_{ik}}^{Carson}(\omega) = \frac{j\omega\mu_0}{\pi} \int_0^\infty \frac{e^{-2(h_i+h_k)u} \cos(b_{ik}u)}{\sqrt{u^2 + j\omega\mu_0\sigma_g} + u}\, \mathrm{d}u \tag{2.31b}$$

Due to the complexity of obtaining numerical results of the infinite integral terms in Equations (2.31a) and (2.31b), Carson has expanded the integrals to infinite series. The ground impedance matrix can then be represented by Carson's correction terms:

$$Z_{ground}(\omega) = \Delta R' + j\Delta X' \tag{2.32}$$

Carson's correction terms for earth return effects are a function of the angle θ ($\theta = 0$ for self impedance and $\theta = \theta_{ik}$ in Fig. 2.1 for mutual impedance) and of the parameter a, which is given by [39]:

$$a = 4\pi \times 10^{-4} D\sqrt{5f\sigma_g} \tag{2.33}$$

where $D = 2h_i$ for the self impedance and $D = D_{ik}$ for the mutual impedance.

Carson presented an infinite integral for the calculation of the terms $\Delta R'$ and $\Delta X'$, developed as an infinite series of trigonometric terms. Carson's correction terms, which are given in [Ω/km],

can be calculated by [39]:

$$\begin{aligned}\Delta R' = 4\omega 10^{-4} \big\{ &\pi/8 - b_1 a\cos\theta + b_2 \left[\left(c_2 - \ln a\right) a^2 \cos 2\theta + \theta a^2 \sin 2\theta \right] \\ &+ b_3 a^3 \cos 3\theta - d_4 a^4 \cos 4\theta - b_5 a^5 \cos 5\theta + b_6 \left[\left(c_6 - \ln a\right) a^6 \cos 6\theta \right. \\ &\left. + \theta a^6 \sin 6\theta \right] + b_7 a^7 \cos 7\theta - d_8 a^8 \cos 8\theta - \ldots \big\}\end{aligned} \tag{2.34a}$$

$$\begin{aligned}\Delta X' = 4\omega 10^{-4} \big\{ &0.5\left(0.6159315 - \ln a\right) + b_1 a\cos\theta - d_2 a^2 \cos 2\theta + b_3 a^3 \cos 3\theta \\ &- b_4 \left[\left(c_4 - \ln a\right) a^4 \cos 4\theta + \theta a^4 \sin 4\theta \right] + b_5 a^5 \cos 5\theta - d_6 a^6 \cos 6\theta \\ &+ b_7 a^7 \cos 7\theta - b_8 \left[\left(c_8 - \ln a\right) a^8 \cos 8\theta + \theta a^8 \sin 8\theta \right] + \ldots \big\}\end{aligned} \tag{2.34b}$$

Each four successive terms of Equations (2.34a) and (2.34b) form a repetitive pattern. The coefficients b_i, c_i and d_i are constants and can be obtained from recursive formulas, as follows [39]:

$$b_i = b_{i-2} \frac{sign}{i(i+2)} \tag{2.35a}$$

$$c_i = c_{i-2} + \frac{1}{i} + \frac{1}{i+2} \tag{2.35b}$$

$$d_i = \frac{\pi}{4} b_i \tag{2.35c}$$

where $b_1 = \frac{\sqrt{2}}{6}$, $b_2 = \frac{1}{16}$ and $c_2 = 1.3659315$. $sign$ is changing after four successive terms: $sign = +1$ for $i = 1, 2, 3, 4; 9, 10, 11, 12; \ldots$ and $sign = -1$ for $i = 5, 6, 7, 8; 13, 14, 15, 16; \ldots$.

The infinite series quickly converges at low frequencies, but the convergence decreases as frequency increases leading to truncation errors. This problem motivated a series of subsequent research in order to find simpler solutions with less approximations for the ground impedance. Some of these work can be found in [39–43] among others.

A closed-form approximation to Carson's integrals has been proposed by Deri et al. in [41], which is easier to solve, but it is still being affected by the high frequency drawbacks, like in Carson's

equations. Deri's expressions are given by:

$$z_{g_{ii}}^{Deri}(\omega) = \frac{j\omega\mu_0}{2\pi} \ln\left(\frac{h_i + p}{h_i}\right) \tag{2.36a}$$

$$z_{g_{ik}}^{Deri}(\omega) = \frac{j\omega\mu_0}{2\pi} \ln\left(\frac{D"_{ik}}{D'_{ik}}\right) \tag{2.36b}$$

where

$$p = (j\omega\mu_0\sigma_g)^{-1/2} \tag{2.37a}$$

$$D"_{ik} = \sqrt{b_{ik}^2 + (h_i + h_k + 2p)^2} \tag{2.37b}$$

$$D'_{ik} = \sqrt{b_{ik}^2 + (h_i + h_k)^2} \tag{2.37c}$$

and p is the complex penetration depth.

Except for the formulation presented in [40], the other formulations presented in [7,41,42] do not consider the displacement current in the ground. This assumption is not valid for higher frequencies, considering that the displacement current becomes comparable to the conduction current in the ground.

Respecting the conditions of applicability and limitations, the formulas that consider $\omega\varepsilon_g = 0$, may be used replacing σ_g by $\sigma_g + j\omega\varepsilon_g$, where ε_g is the permittivity of the ground.

Thus, for a generic line with n phases where each phase consists of one conductor, the ground impedance matrix can be written as:

$$[Z_g(\omega)] = \begin{bmatrix} z_{g_{11}} & z_{g_{12}} & \cdots & z_{g_{1n}} \\ z_{g_{21}} & z_{g_{22}} & \cdots & z_{g_{2n}} \\ \vdots & \vdots & \ddots & \vdots \\ z_{g_{n1}} & z_{g_{n2}} & \cdots & z_{g_{nn}} \end{bmatrix} \tag{2.38}$$

With the calculation of the external, internal and ground impedances, now it is possible to find

the total longitudinal impedance of the line as given in Equation (2.1).

2.1.2 Transverse Admittance of the Line

The transverse admittance of a transmission line is composed of a conductance and a capacitance. Since in commonly used formulations employed in power system transient simulation, the effect of shunt conductance is assumed to be very small, it can therefore be neglected [11, 44]. For this reason, only the calculation of the capacitance matrix will be described.

The relation of the total charge per-unit-length on a given conductor and all the voltages inducing such charge is given by the capacitance matrix C [2]:

$$[Q] = [C][V] \tag{2.39}$$

or in expanded form:

$$\begin{bmatrix} q_1 \\ q_2 \\ \vdots \\ q_n \end{bmatrix} = \begin{bmatrix} \sum_{k=1}^{n} c_{1k} & -c_{12} & \cdots & -c_{1n} \\ -c_{21} & \sum_{k=1}^{n} c_{2k} & \cdots & -c_{2n} \\ \vdots & \vdots & \ddots & \vdots \\ -c_{n1} & -c_{n2} & \cdots & \sum_{k=1}^{n} c_{nk} \end{bmatrix} \begin{bmatrix} V_1 \\ V_2 \\ \vdots \\ V_n \end{bmatrix} \tag{2.40}$$

where $C_{ij} = C_{ji}$ because C is a symmetric matrix, regardless of whether the surrounding medium is homogeneous or inhomogeneous.

The value of C_{ij} can be obtained by setting all voltages except V_j to zero and then determining the charge q_i:

$$C_{ij} = \left.\frac{q_i}{V_j}\right|_{V_1=\cdots=V_{j-1}=Vj+1=\cdots=V_n=0} \tag{2.41}$$

This is a very straightforward method to calculate the capacitance for a multiconductor transmission line. However, there is a simpler method which consists on applying a per-unit-length charge q_j on conductor j, the negative equivalent charge $-q_j$ on the reference conductor and zero charge on the remaining conductors and then determining the voltage between conductor i and the

reference conductor.

This alternative method is achieved inverting Equations (2.39) and (2.40), resulting in:

$$[V] = [P][Q] \tag{2.42}$$

or in expanded form:

$$\begin{bmatrix} V_1 \\ V_2 \\ \vdots \\ V_n \end{bmatrix} = \begin{bmatrix} p_{11} & p_{12} & \cdots & p_{1n} \\ p_{21} & p_{22} & \cdots & p_{2n} \\ \vdots & \vdots & \ddots & \vdots \\ p_{n1} & p_{n2} & \cdots & p_{nn} \end{bmatrix} \begin{bmatrix} q_1 \\ q_2 \\ \vdots \\ q_n \end{bmatrix} \tag{2.43}$$

The entries in P are known as the coefficients of potential, and p_{ij} can be calculated similarly as C_{ij} was calculated in Equation (2.41). So, from Equation (2.43):

$$p_{ij} = \left.\frac{V_i}{q_j}\right|_{q_1=\cdots=q_{j-1}=qj+1=\cdots=q_n=0} \tag{2.44}$$

Once the matrix P is obtained, C can easily be calculated by:

$$[C] = [P]^{-1} \tag{2.45}$$

It is important to highlight that the self-capacitance between the conductor i and the reference conductor, c_{ii} , is not simply the value of C_{ij} in Equation (2.40). For instance, the value of C_{ij} is the negative of the mutual capacitance between two conductors, while the value of C_{ii} is the sum of the self-capacitance of conductor i and the mutual capacitances in that row (or column). In other words, to obtain the self-capacitance c_{ii}, it is necessary to add all the values in the row (or column) i of C.

And finally, the admittance matrix can be determined by the following expression:

$$[Y] = j\omega[C] \tag{2.46}$$

2.2 Underground Coaxial Cables

2.2.1 Longitudinal Impedance of the Coaxial Cable

The impedance of a coaxial cable can be derived from the analytical field solution [3]. Fig. 2.3 represents a generic coaxial cable with k cylindrical conductors.

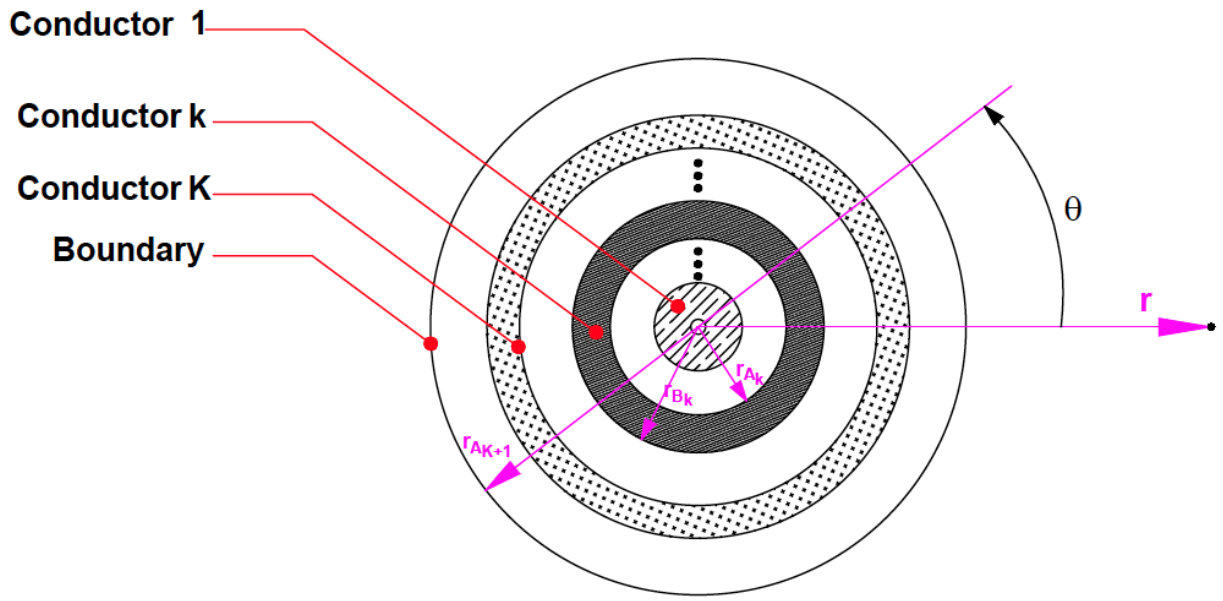

Fig. 2.3: Geometry of a generic coaxial cable [3].

where r_{A_k} and r_{B_k} are the internal and external radii of the k^{th} conductor respectively.

The longitudinal electric field (E) in cylindrical coordinates inside the k^{th} conductor is given by [3]:

$$E(r) = \frac{\sqrt{j\omega\sigma_k\mu_k}}{\sigma_k}\left[C_{I_k} I_0\left(r\sqrt{j\omega\sigma_k\mu_k}\right) - C_{K_k} K_0\left(r\sqrt{j\omega\sigma_k\mu_k}\right)\right] \tag{2.47}$$

where:

$$C_{I_k} = \frac{1}{2\pi C_{D_k}}\left[\frac{I_{A_k}}{r_{A_k}} K_1\left(r_{B_k}\sqrt{j\omega\sigma_k\mu_k}\right) + \frac{I_{B_k}}{r_{B_k}} K_1\left(r_{A_k}\sqrt{j\omega\sigma_k\mu_k}\right)\right]$$

$$C_{K_k} = \frac{-1}{2\pi C_{D_k}} \left[\frac{I_{A_k}}{r_{A_k}} I_1 \left(r_{B_k} \sqrt{j\omega\sigma_k\mu_k} \right) + \frac{I_{B_k}}{r_{B_k}} I_1 \left(r_{A_k} \sqrt{j\omega\sigma_k\mu_k} \right) \right]$$

$$C_{D_k} = I_1 \left(r_{B_k} \sqrt{j\omega\sigma_k\mu_k} \right) K_1 \left(r_{A_k} \sqrt{j\omega\sigma_k\mu_k} \right) - I_1 \left(r_{A_k} \sqrt{j\omega\sigma_k\mu_k} \right) K_1 \left(r_{B_k} \sqrt{j\omega\sigma_k\mu_k} \right)$$

I_{A_k} and I_{B_k} are, respectively, the internal and external return currents of the k^{th} conductor. I_n is the n^{th} order Bessel Function of the first kind and K_n is the n^{th} order Bessel Function of the second kind.

The electric field on the internal and external surfaces of a given conductor can be derived as [45]:

$$E(r_{A_k}) = Z_{A_k} I_{A_k} + Z_{M_k} I_{B_k} \tag{2.49a}$$

$$E(r_{B_k}) = Z_{M_k} I_{A_k} + Z_{B_k} I_{B_k} \tag{2.49b}$$

where:

$$\begin{aligned} Z_{A_k} = \frac{\sqrt{j\omega\sigma_k\mu_k}}{2\pi r_{A_k}\sigma_k C_{D_k}} \Big[& I_0 \left(r_{A_k} \sqrt{j\omega\sigma_k\mu_k} \right) K_1 \left(r_{B_k} \sqrt{j\omega\sigma_k\mu_k} \right) \\ & + K_0 \left(r_{A_k} \sqrt{j\omega\sigma_k\mu_k} \right) I_1 \left(r_{B_k} \sqrt{j\omega\sigma_k\mu_k} \right) \Big] \end{aligned} \tag{2.50a}$$

$$\begin{aligned} Z_{B_k} = \frac{\sqrt{j\omega\sigma_k\mu_k}}{2\pi r_{B_k}\sigma_k C_{D_k}} \Big[& I_0 \left(r_{B_k} \sqrt{j\omega\sigma_k\mu_k} \right) K_1 \left(r_{A_k} \sqrt{j\omega\sigma_k\mu_k} \right) \\ & + K_0 \left(r_{B_k} \sqrt{j\omega\sigma_k\mu_k} \right) I_1 \left(r_{A_k} \sqrt{j\omega\sigma_k\mu_k} \right) \Big] \end{aligned} \tag{2.50b}$$

$$Z_{M_k} = \frac{1}{2\pi r_{A_k} r_{B_k} \sigma_k C_{D_k}} \tag{2.50c}$$

First, the impedance of the coaxial cable will be determined without considering the earth return effect, assuming that the system in Fig. 2.3 has a perfect electric conductor (PEC) surface at $r_{A_{k+1}}$, so this surface can be used as the reference voltage and the current return path for the conductors. With this under consideration, the series impedance matrix for a generic coaxial cable

can be written as:

$$[Z] = \begin{bmatrix} Z_1^d & Z_2^{od} & Z_3^{od} & \cdots & Z_K^{od} \\ Z_2^{od} & Z_2^d & Z_3^{od} & \cdots & Z_K^{od} \\ Z_3^{od} & Z_3^{od} & Z_3^d & \cdots & Z_K^{od} \\ \vdots & \vdots & \vdots & \ddots & \vdots \\ Z_K^{od} & Z_K^{od} & Z_K^{od} & \cdots & Z_K^d \end{bmatrix} \tag{2.51}$$

where:

$$Z_i^d = \sum_{k=i}^{K} Z_{EQ_k} - 2 \sum_{k=i+1}^{K} Z_{M_k} \tag{2.52a}$$

$$Z_i^{od} = \sum_{k=i}^{K} Z_{EQ_k} - Z_{M_i} - 2 \sum_{k=i+1}^{K} Z_{M_k} \tag{2.52b}$$

$$Z_{EQ_k} = Z_{B_k} + Z_{D_k} + Z_{A_{k+1}} \tag{2.52c}$$

$$Z_{EQ_K} = Z_{B_K} + Z_{D_K} \tag{2.52d}$$

$$Z_{D_k} = \frac{j\omega\mu_0}{2\pi} \ln\left(\frac{r_{A_{k+1}}}{r_{B_k}}\right) \tag{2.52e}$$

At last, the component representing the ground impedance will be calculated in order to find the total longitudinal impedance of the coaxial cable. The electric field of coaxial cables buried close to the surface of the earth can be determined substituting the cable with a current filament. In this case, the electric field in the earth can be calculated as [38]:

$$\begin{aligned} E_g = & -\frac{j\omega\mu_g I}{2\pi} \left[K_0\left(\frac{D}{p_g}\right) - K_0\left(\frac{D'}{p_g}\right) \right. \\ & \left. + \int_0^\infty \frac{2e^{(y-h)\sqrt{\alpha^2 + 1/p_g^2}}}{\frac{\mu_g}{\mu_0}\alpha + \sqrt{\alpha^2 + 1/p_g^2}} \cos(x\alpha)\, \mathrm{d}\alpha \right] \end{aligned} \tag{2.53}$$

where:

$$D = \sqrt{x^2 + (y+h)^2}$$

$$D' = \sqrt{x^2 + (y-h)^2}$$

$$p_g = \frac{1}{\sqrt{j\omega\mu_g\sigma_g}}$$

I is the current in the filament, h is the burial depth of the cable, μ_g and σ_g are, respectively, the magnetic permeability and the conductivity of the ground. x and y are the coordinates of the point on the surface of the cable, where the electric field is going to be calculated. p_g is the complex penetration depth in the earth, which is related to the real penetration depth (δ) by:

$$\delta = \sqrt{2}|p| \tag{2.55}$$

The ground impedance is defined as [3]:

$$Z_g = \frac{E_g}{I} \tag{2.56}$$

which, assuming that the electric field is the same at any point of the surface ($x = r_c$ and $y = -h$), results in [38]:

$$\begin{aligned} Z_g = & -\frac{j\omega\mu_g}{2\pi}\left[K_0\left(\frac{r_c}{p_g}\right) - K_0\left(\frac{\sqrt{r_c^2+4h^2}}{p_g}\right)\right. \\ & \left. + \int_0^\infty \frac{2e^{-2h\sqrt{\alpha^2+1/p_g^2}}}{\frac{\mu_g}{\mu_0}\alpha + \sqrt{\alpha^2+1/p_g^2}}\cos\left(r_c\alpha\right)\mathrm{d}\alpha\right] \end{aligned} \tag{2.57}$$

and r_c is the radius of the coaxial cable. Pollaczek was the first to derive Equation (2.57), and for this reason, it is also called the "Pollaczek's formula" [3].

However, if the coaxial cable is deeply buried in the ground ($h \gg \delta_g$), the ground impedance can be derived from Equation (2.50a) assuming that the earth becomes a coaxial conductor with infinite outer radius, *i.e.*, $r_{A_k} = r_c$ and $r_{B_k} \to \infty$, resulting in:

$$Z_g = \frac{\sqrt{j\omega\mu_g/\sigma_g}}{2\pi r_c}\frac{K_0\left(r_c/p_g\right)}{K_1\left(r_c/p_g\right)} \tag{2.58}$$

Now that the ground impedance is known, the total longitudinal impedance can be calculated with Equation (2.51) by modifying Equation (2.52d) into:

$$Z_{EQ_K} = Z_{B_K} + Z_{D_K} + Z_g \tag{2.59}$$

2.2.2 Transverse Admittance of the Coaxial Cable

For the same reasons presented in Section 2.1.2, only the calculation of the capacitance matrix will be described using the notations given in Section 2.2.1. Fig. 2.3 shows a generic coaxial cable with K insulations and the per-unit-length capacitance related to the insulation between conductors k and $k+1$ is given by [46]:

$$C_{in_k} = \frac{2\pi\varepsilon_k}{\ln\left(\frac{r_{A_{k+1}}}{r_{B_k}}\right)} \qquad (k = 1, 2, \cdots, K) \tag{2.60}$$

where ε_k is the permittivity of the k^{th} insulation. The capacitance matrix for a generic coaxial cable only has three diagonals and can be written as [3]:

$$[C] = \begin{bmatrix} C_1^d & C_2^{od} & 0 & 0 & 0 & 0 \\ C_2^{od} & C_2^d & C_3^{od} & 0 & 0 & 0 \\ 0 & C_3^{od} & C_3^d & C_4^{od} & 0 & 0 \\ 0 & 0 & \ddots & \ddots & \ddots & 0 \\ 0 & 0 & 0 & C_{K-1}^{od} & C_{K-1}^d & C_K^{od} \\ 0 & 0 & 0 & 0 & C_K^{od} & C_K^d \end{bmatrix} \tag{2.61}$$

where:

$$C_1^d = C_{in_1}$$

$$C_k^d = C_{in_{k-1}} + C_{in_k} \qquad (k = 2, 3, \cdots, K)$$

$$C_k^{od} = -C_{in_{k-1}} \qquad (k = 2, 3, \cdots, K)$$

Once the per-unit-length capacitance matrix is calculated, it is possible to obtain the admittance matrix using Equation (2.46).

2.3 Summary

In this chapter, the assumptions and the analytical equations to obtain the per-unit-length resistance, inductance and capacitance of arbitrary transmission lines (overhead lines and underground cables) were discussed. Next chapter will provide some background theory, including the equations that govern the electric and magnetic fields and the methods available to solve such equations.

Chapter 3

Background Theory

In order to calculate the electrical parameters of transmission lines using numerical methods, it is necessary to find the quasi-static solution of electric and magnetic fields in the two-dimensional cross section of these configurations [3]. The solution of the quasi-magnetic and the quasi-electric problems are used to calculate the series impedance (resistance and inductance) and the shunt admittance (capacitance) matrices, respectively. It is more difficult to handle the quasi-static magnetic fields due to the frequency dependence, and consequently the skin and proximity effects. The electromagnetic field equations will be discussed in Section 3.1.

There are a number of methods that can be used to solve the quasi-static magnetic fields including the subdivision method, finite element method (FEM), boundary element method (BEM), among others. The subdivision method, just like the name indicates, consists of dividing the conductors of a multiconductor transmission line into N subconductors such that the current density can be assumed as uniform over the cross section of each of the subconductors, simplifying the problem to a set of linear equations [47]. The problem with this method arises when the effects of frequency dependence are strong, in such case it is necessary to use a large number of very small subconductors to account for the assumption of uniform current density and to obtain accurate results.

The boundary element method can handle open boundary problems easier than other methods, because only the boundary is discretized instead of the whole domain, speeding up the simulation. But it may be more difficult to apply this method when the earth return effects are considered [3].

The most fundamental concept of the finite element method is that any continuous function can be approximated by a model consisting of a set of continuous functions (within a range) defined over a finite number of sub-domains, or finite elements [48]. In this thesis, the finite element method will be applied to calculate the series impedance and capacitance matrices of a transmission line. Section 3.2 will give more details about this technique.

According to what was discussed in Section 2.1.1, the earth must be included in the calculation of transmission lines parameters. Considering that the skin depth of the ground is very large, specially at low frequencies, it would be complicated to solve the whole region using finite element method alone.

There are several techniques for handling open boundary problems [16], some of the most important methods can be categorized under the following five groups: truncation of outer boundaries; ballooning; infinite or mapped elements; spatial transformation; and coupling finite element method with an analytical method or other numerical method.

The truncation of outer boundaries is used to limit the area of interest up to where the field becomes negligible, this means that the potential or the normal derivative of the potential will be close to zero. The problem is that this truncation boundary, sometimes can be very large, specially in the low frequency range when the skin depth of the ground becomes an issue, resulting in more elements to mesh the solution region, and consequently, increased memory requirements and computation time. Furthermore, the space truncation may produce unacceptable errors in the calculation of the transmission line parameters [17].

The ballooning technique consists of surrounding the interior region by an annular region defined by a mesh of super finite elements. Then new annulus are added using a recursive process in which the inner nodes overlap the outer nodes of the previous annulus. By doing so, the radius

of the outer boundary increases in a geometric progression and the system rapidly converges. This technique is a significant improvement over the truncation of the outer boundary method. The problem is that it can be problematic to apply symmetry conditions and get the results in the outer region [17, 22].

In the case of infinite element technique using mapped finite elements, the domain of a regular finite element is transformed into an infinite domain through a singular mapping function. Since the field variables are still described by the regular finite element interpolation functions, the mapping function is used only for the Jacobian transformation. [17, 26]

Whereas the infinite element technique transforms a finite domain to an infinite domain, the spatial transformation (mapping or transformation scheme) converts a physical unbounded space to a finite domain using a geometrical mapping method. Conformal mapping can be employed for the calculation of axi-symmetric open boundary and waveguide problems [30, 31]. The important feature of conformal mapping is that the governing equation in static electric and magnetic problems (Poisson's equation) remains unchanged [49]. In most cases, the post-processing formulations, which are usually used to calculate the distributed parameters in the case of a transmission line, also remain unchanged or require a factor that is a function of the mapping. For this reason, the conformal mapping method has been chosen to approach the problem in this thesis, more details about this technique will be given in Section 3.3.

3.1 Electromagnetic Field Equations

The behaviour of electric and magnetic fields is governed by Maxwell's equations, which in the frequency domain ($e^{j\omega t}$ dependence), and assuming there is no free charge, are given by:

$$\nabla \times \mathbf{E} = -j\omega\mathbf{B} \tag{3.1a}$$

$$\nabla \times \mathbf{H} = \sigma\mathbf{E} + j\omega\mathbf{D} \tag{3.1b}$$

$$\nabla \cdot \mathbf{D} = 0 \tag{3.1c}$$

$$\nabla \cdot \mathbf{B} = 0 \tag{3.1d}$$

where σ is the conductivity of medium. Electric and magnetic fields can be written using the electric scalar potential (V), and the magnetic vector potential ($\mathbf{A}$), as:

$$\mathbf{E} = -\nabla V - j\omega\mathbf{A} \tag{3.2a}$$

$$\mathbf{B} = \nabla \times \mathbf{A} \tag{3.2b}$$

Combining Equations (3.1b), (3.2a) and (3.2b) and considering that $\mathbf{B} = \mu\mathbf{H}$ and $\mathbf{D} = \varepsilon\mathbf{E}$ yields:

$$\nabla \times \frac{1}{\mu}\nabla \times \mathbf{A} + (\sigma + j\omega\varepsilon)(j\omega\mathbf{A} + \nabla V) = 0 \tag{3.3}$$

Taking the divergence of Equation (3.2a) and using Coulomb's Gauge ($\nabla \cdot A = 0$) results in [16]:

$$\nabla^2 V = 0 \tag{3.4}$$

which is simply the Laplace equation. Equations (3.3) and (3.4) are the governing equations of the problem. It is worth mentioning that Equations (3.2a) and (3.4) are valid for homegeneous medium only.

The method described so far is valid for the general form of the Helmholtz equation. Some approximations will be introduced in the following Sections.

3.1.1 Quasi-Stationary Approximation

The quasi-stationary approximations of the Helmholtz equation, for the electric and magnetic cases, are considered appropriate to solve the field problem for frequencies in which the electrical wavelengths are greater than approximately ten times the critical dimensions of the cross section

[49]. The quasi-magnetic approximation, considering only the longitudinal current is employed to calculate the per-unit-length resistance matrix (**R**) and inductance matrix (**L**), while the quasi-electric approximation, considering only the in-plane current is used to determine the per-unit-length capacitance matrix (**C**).

Quasi-Magnetic Formulation

Under the two-dimensional quasi-stationary assumption and considering a symmetric and uniform structure along the z axis, the per-unit-length resistance and inductance are associated with the longitudinal component of the current. For that reason, it is assumed that the electric currents of the conductors flow only in the z direction, which can be understood as:

$$\mathbf{A} = A_z \hat{\mathbf{a}}_z \tag{3.5}$$

where $\hat{\mathbf{a}}_z$ is the unit vector pointing in the direction of z.

As a result, only the z component of Equation (3.3) is considered in the quasi-magnetic formulation. Under this assumption, the electric scalar potential (V) remains unchanged in the x-y plane and it varies linearly with z [50]. In other words, the z component of ∇V $\left(\frac{\partial V}{\partial z}\right)$ is a constant. In this thesis, ΔV is used to represent the z component of ∇V, which simply represents the excitation voltage per unit length. With these considerations, and neglecting the displacement current, the governing equation given in Equation (3.3) reduces to:

$$\frac{1}{\mu}\nabla_t^2 A_z + (\omega^2\varepsilon - j\omega\sigma)A_z = \sigma\Delta V = J_z^{ex} \tag{3.6}$$

where, the external excitation current (J_z^{ex}) is nonzero only in metallic conductors, and:

$$\nabla_t^2 = \frac{\partial^2}{\partial x^2} + \frac{\partial^2}{\partial y^2} \tag{3.7}$$

Quasi-Electric Formulation

As mentioned before, under the two-dimensional quasi-electric assumption, only the in-plane current is considered. In other words, it is assumed that the electric current flows only in the x-y plane. Furthermore, for frequencies at which the skin-depth in the ground is much larger than the transmission line cross section geometry, the Faraday's Law given in Equation (3.1a) reduces to:

$$\nabla \times \mathbf{E} = 0 \tag{3.8}$$

that results in:

$$\mathbf{E} = -\nabla V \tag{3.9}$$

Equation (3.1c) can be rewritten as:

$$\nabla \cdot (\varepsilon \mathbf{E}) = 0 \tag{3.10}$$

Now, substituting Equation (3.9) into Equation (3.10) yields:

$$\nabla \cdot (-\varepsilon \nabla V) = 0 \tag{3.11}$$

Equation (3.11) can be expanded as:

$$\nabla \varepsilon \cdot \nabla V + \varepsilon \nabla \cdot (\nabla V) = 0 \tag{3.12}$$

And finally, the governing equation for the quasi-electric formulation for the two-dimensional in-plane excitation is given by:

$$\nabla \varepsilon \cdot \nabla V + \varepsilon \nabla^2 V = 0 \tag{3.13}$$

Equations (3.6) and (3.13) are the governing equations of the quasi-magnetic and quasi-electric assumptions, respectively.

3.2 Finite Element Method

The basic technique of the finite element method appeared sometime in 1941 when Hrenikoff presented the solution of a problem of elasticity using the "frame work method". Later, in 1960, the term finite element was designated by Clough [51].

The FEM is a mathematical method for solving partial differential equations, such as Poisson and Laplace equations. The most fundamental concept of the finite element method is that any continuous function can be approximated by a model consisting of a set of continuous functions (within a range) defined over a finite number of sub-domains, or finite elements [48]. Each finite element is made up of nodes, which are the points where the edges of the element meet.

Unlike other methods that were used in the past, the FEM has only practical benefit if it is associated with a digital computer. This requirement is due to the large amount of calculations required to be undertaken, especially in solving large systems of linear equations. One can understand why the rapid development of the FEM has practically coincided with the widespread use of computers in research centres. With the proliferation of microcomputers, which occurred in the late 80s and in the 90s, the FEM finally reaches the hands of most engineers.

For purposes of this thesis, FEM analysis will be accomplished with the aid of a commonly used commercial finite element analysis software program, COMSOL Multiphysics [52].

3.3 Conformal Mapping

A complex analytic function $f(\zeta)$ can be interpreted as a mapping or transformation function that takes a point $z = x + jy$ which belongs to a given domain $\Omega \subset \mathbb{C}$ to a point $w = u + jv$ which belongs to the mapped domain $D \subset \mathbb{C}$. The transformed space (D) can assume different geometries, however, the unit circle, as shown in Fig. 3.1, is the only case that presents an explicit solution of the Poisson equation [53].

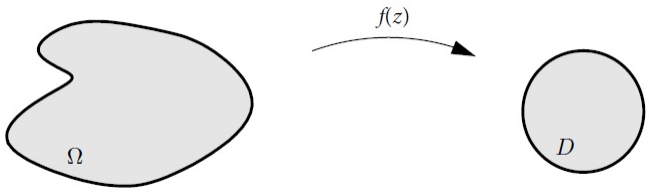

Fig. 3.1: Mapping to the unit circle.

A mapping function is called conformal if, and only if, it is one to one, *i.e.*, each point $w \in D$ comes from a unique point $z \in \Omega$ and the inverse function $f^{-1}(z)$ is a well defined map from D back to Ω. Furthermore, a conformal mapping is capable of preserving the angles in the Euclidean plane [54].

A bilinear transformation is a conformal mapping scheme, which has been effectively employed for the solution of the Laplace equation by converting a semi-open half-space problem to an equivalent closed region [49]. This scheme maps the half-space ($y > 0$) to the interior of a unit circle and is applicable to planar transmission lines over a perfectly conducting infinite ground plane. Another characteristic of the bilinear transformation is that a circular geometry in the original domain will remain a circle in the mapped space, this is proved in Appendix B.

In this thesis, a two-dimensional conformal transformation scheme is used to obtain the parameters of an arbitrary overhead transmission line in an unbounded lossy space. This scheme is a generalization of bilinear transformation for solving full-space unbounded problems. This method consists of dividing an unbounded two-dimensional space into two half-spaces and each half-space is mapped to a unit circle with coinciding boundaries.

The bilinear mapping $f(z)$, that transforms the upper half-space ($y > 0$) in Cartesian coordinates to a unit circle is given by [49]:

$$f(z) = \frac{1 + jz}{1 - jz} \tag{3.14}$$

where z, as mentioned before, is a point in the complex plane.

In order to map the lower half-space ($y < 0$) to the second unit circle, the lower space should be mapped to the upper space first (y is replaced by $-y$), and then the same mapping scheme can be applied. This is achieved by replacing z by its complex conjugate z^*.

Mathematically, the two mapped circles are now coincident, but numerical solution of the problem requires the circles to be separated. For this reason, and for getting the same coordinates convention (*i.e.*, when a given point in the original space is mapped to the unit circle, the sign of the coordinates will remain the same), the two circles are translated and rotated such that the circle representing the upper half-space ($y > 0$) is adjacent to the circle representing the lower half-space ($y < 0$) with both circles touching each other at the origin. The points related to infinity are located at the top of the upper circle and the bottom of the lower circle. The interface between the upper and lower spaces ($y = 0$) is the common boundary of the two regions and it is mapped to the boundary of both circles. The proposed mapping is achieved by using the following mapping functions for the upper half-space ($y > 0$):

$$w_1 = u_1 + jv_1 = f_1(z) = -j[f(z) - 1] = \frac{2z}{1 - jz} \tag{3.15}$$

or:

$$u_1(x, y) = \frac{2x}{x^2 + (1 + y)^2} \tag{3.16a}$$

$$v_1(x, y) = \frac{2(x^2 + y + y^2)}{x^2 + (1 + y)^2} \tag{3.16b}$$

and, for the lower half-space ($y < 0$):

$$w_2 = u_2 + jv_2 = f_2(z) = j[f^*(z^*) - 1] = \frac{2z}{1 + jz} \tag{3.17}$$

or:

$$u_2(x, y) = \frac{2x}{x^2 + (1 - y)^2} \tag{3.18a}$$

$$v_2(x,y) = \frac{2(-x^2 + y - y^2)}{x^2 + (1-y)^2} \tag{3.18b}$$

Here, w_1 represents a point in the upper mapped half-space ($v > 0$) and w_2 represents a point in the lower mapped half-space, in which u_i and v_i are the real and imaginary parts, respectively. Equations (3.16) and (3.18) can be rewritten to calculate u and v for any value of y (positive or negative):

$$u(x,y) = \frac{2x}{x^2 + (1+|y|)^2} \tag{3.19a}$$

$$v(x,y) = \text{sgn}(y)\frac{2[|y| + (x^2+y^2)]}{x^2 + (1+|y|)^2} \tag{3.19b}$$

In order to better understand the mapping effect, Fig. 3.2 illustrate the original space with some lines parallel to the abscissa and ordinate axes, represented in blue and red, respectively, which then are mapped using Equation (3.19) and shown in Fig. 3.3.

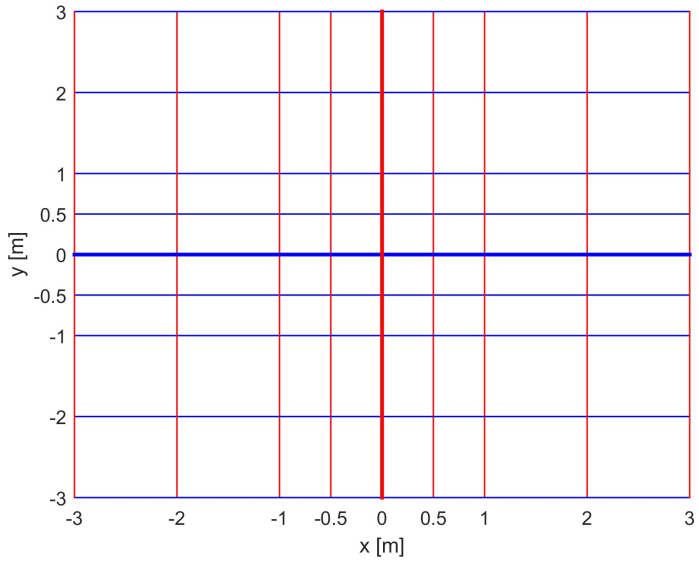

Fig. 3.2: Lines parallel to the abscissa and ordinate axes in the original space.

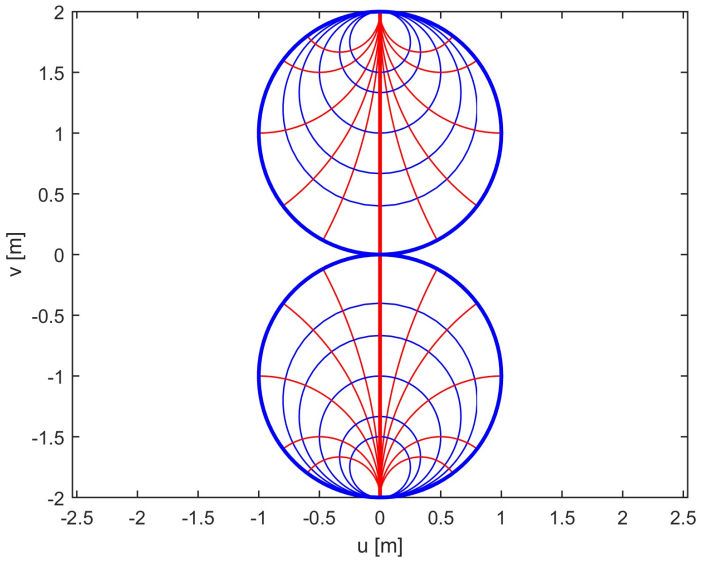

Fig. 3.3: Lines parallel to the x and y axes in the mapped space.

Due to conformality of the transformation, the value of a scalar potential at each point in the original space remains unchanged in the equivalent point in the mapped space and the governing equations remain the same or just modified by a simple mapping factor.

3.4 Summary

Section 3.1 introduced the electric and magnetic field equations and the assumptions and approximations used to simplify the problem. Section 3.2 gave a brief description of the finite element method, which was chosen to solve the partial differential equations. And Section 3.3 gave further information regarding the conformal mapping, which is used to convert a physical unbounded domain into a finite domain. All the theory seen in this chapter will be addressed in the next chapter, where all these techniques will be put together to extract the per-unit-length parameters of a transmission line.

Chapter 4

Proposed Method - Parameters Extraction using Conformal Mapping and Finite Elements

This chapter will exploit the theory given in Chapter 3 to find the solution of the partial differential equations that govern the electromagnetic fields using the finite element method, and applying the conformal mapping technique to handle the problem of simulating unbounded domains. And culminating with the extraction of the electric parameters (resistance, inductance and capacitance) of an overhead transmission line or underground cable.

Before proceeding, it is necessary to determine the mapping factor (M) to modify the governing equations given by Equations (3.6) and (3.13). As seen in Equation (3.7), to find the first modified governing equation in the mapped space, it is necessary to find the second order partial derivatives of a given function, which in this case is the z-component of the magnetic vector potential. A complex function $f(z) = u(x, y) + jv(x, y)$, where $z = x + jy$, has a complex derivative $f'(z)$ if, and only if, its real and imaginary components are continuously differentiable and satisfy the Cauchy-Riemann equations [54].

Also, it is necessary to find the solution of the dot product between the gradient of two functions to find the second modified governing equation in the mapped space.

The Cauchy-Riemann equations, the definition of the mapping factor and the derivation of the dot product between the gradient of two functions are given in details in Appendix A. So, from Equation (A.2) it is possible to obtain the formula for the mapping factor, in the original domain, as:

$$M = \frac{2}{x^2 + (1 + |y|)^2} \tag{4.1}$$

The mapping factor, in the mapped domain, is given by:

$$M = \frac{u^2 + (|v| - 2)^2}{2} \tag{4.2}$$

Now, it is possible to use Equation (A.9) in (3.6) to obtain the governing equation in the mapped space:

$$\frac{M^2}{\mu}\nabla_t^2 A_z^T + (\omega^2 \varepsilon^T - j\omega\sigma^T)A_z^T = J_z^{Tex} \tag{4.3}$$

Equation (4.3) is the case of homogeneous conductivity ($\sigma^T = \sigma$) and permittivity ($\varepsilon^T = \varepsilon$). The electric properties of the medium can be modified to include the mapping factor in order to maintain the format of the original equation which will be solved in COMSOL Multiphysics:

$$\frac{1}{\mu}\nabla_t^2 A_z^T + (\omega^2 \varepsilon^T - j\omega\sigma^T)A_z^T = J_z^{Tex} \tag{4.4}$$

where A_z^T, ε^T, σ^T, J_z^{Tex} are the z component of the magnetic vector potential, the permittivity, the conductivity and the external current density, respectively, all in the mapped space. The modification to the electric properties of the medium in the mapped space are as follows:

$$\varepsilon^T = \frac{\varepsilon}{M^2} \tag{4.5a}$$

$$\sigma^T = \frac{\sigma}{M^2} \tag{4.5b}$$

Now, the governing equation given by Equation (4.4) is the quasi-stationary approximation of the Helmholtz scalar wave equation, but unlike in Equation (3.6), it is over a nonhomogeneous medium in terms of conductivity and permittivity in the mapped space, as it can be observed in Equations (4.5a) and (4.5b). Note that permeability remains homogeneous ($\mu^T = \mu$).

The second governing equation in the mapped space can be derived from Equation (3.13) taking into account Equations (A.9) and (A.13):

$$\left(\nabla\varepsilon^T \cdot \nabla V^T\right) + \varepsilon^T \nabla^2 V^T = 0 \tag{4.6}$$

In this case, the governing equation is independent from the mapping factor.

Due to the assumptions and definitions given in Appendix A, the solution of Equations (4.4) and (4.6) implies that the obtained A_z and V at any arbitrary point (u, v) in the mapped space is the same as the solution of Equations (3.6) and (3.13) at any corresponding point (x, y) in the original space:

$$A_z(x, y) = A_z^T(u, v) \tag{4.7a}$$

$$V(x, y) = V^T(u, v) \tag{4.7b}$$

The solution of the governing equations given by Equations (4.4) and (4.6) are obtained using a commonly used commercial FEM based simulation software program, COMSOL Multiphysics.

As mentioned in the previous chapter, the solution of the static electric and the quasi-static magnetic fields are used to determine the per-unit-length parameters of the transmission line. Specifically, the magnetic field energy is used to calculate the inductance matrix ($\mathbf{L}$), the electric field energy for the capacitance matrix ($\mathbf{C}$), and the conductor resistive losses for the calculation of the resistance matrix ($\mathbf{R}$).

In order to calculate those energies and losses, it is necessary to find the solution for some

surface integrals. In general, any surface integration in the original space (S) can be calculated in the mapped space (S^T) by [16]:

$$\iint_S f(x,y)dxdy = \iint_{S^T} f(u,v)J(u,v)dudv \tag{4.8}$$

where $J(u,v)$ is the Jacobian matrix of the transformation defined as [49]:

$$J(u,v) = \left|\frac{\partial(x,y)}{\partial(u,v)}\right| = \begin{vmatrix} \frac{\partial x}{\partial u} & \frac{\partial x}{\partial v} \\ \frac{\partial y}{\partial u} & \frac{\partial y}{\partial v} \end{vmatrix} \tag{4.9}$$

Applying Equations (A.1a) and (A.1b) to Equation (4.9) yields:

$$J(u,v) = \frac{1}{M^2} \tag{4.10}$$

Applying Equation (4.10) to (4.8) gives the surface integration in the mapped space in terms of the mapping factor, as:

$$\iint_S f(x,y)dxdy = \iint_{S^T} \frac{f(u,v)}{M^2}dudv \tag{4.11}$$

With the background provided in Chapter 3, Appendix A and in the introduction of this Chapter, now it is possible to extract the per-unit-length parameters of a given transmission line. The procedure for obtaining the parameters will be given in the following sections.

4.1 Series Impedance of the Line

This section will describe a procedure for extracting the longitudinal or series impedance of an arbitrary transmission line represented by: Resistance Matrix (**R**) and Inductance Matrix (**L**).

4.1.1 Inductance Matrix

As mentioned before, the magnetic field energy method will be used for the calculation of the self and mutual inductance of the transmission line. The magnetic energy stored in a unit length of the unbounded domain (original space) can be calculated by [49]:

$$W_m = \frac{1}{2}\int_{-\infty}^{+\infty}\int_{-\infty}^{+\infty}\frac{1}{\mu}|\mathbf{B}|^2 dxdy \tag{4.12}$$

Substituting Equation (3.2b) in (4.12) results in:

$$W_m = \frac{1}{2}\int_{-\infty}^{+\infty}\int_{-\infty}^{+\infty}\frac{1}{\mu}|\nabla\times\mathbf{A}|^2 dxdy \tag{4.13}$$

Taking into account Equation (3.5), the curl of the magnetic vector potential ($\nabla\times\mathbf{A}$) results in:

$$\nabla\times\mathbf{A} = \frac{\partial A_z}{\partial y}\hat{\mathbf{a}}_x - \frac{\partial A_z}{\partial x}\hat{\mathbf{a}}_y \tag{4.14}$$

Substituting Equation (4.14) in (4.13) yields:

$$W_m = \frac{1}{2}\int_{-\infty}^{+\infty}\int_{-\infty}^{+\infty}\frac{1}{\mu}\left[\left(\frac{\partial A_z}{\partial x}\right)^2 + \left(\frac{\partial A_z}{\partial y}\right)^2\right] dxdy \tag{4.15}$$

Now, applying the chain rule to Equation (4.15) and then considering Equation (A.3a) results in:

$$\begin{aligned} W_m = \frac{1}{2}\int_{-\infty}^{+\infty}\int_{-\infty}^{+\infty}\frac{1}{\mu}\Bigg[&\left(\frac{\partial A_z^T}{\partial u}\frac{\partial u}{\partial x} + \frac{\partial A_z^T}{\partial v}\frac{\partial v}{\partial x}\right)^2 \\ &+ \left(\frac{\partial A_z^T}{\partial u}\frac{\partial u}{\partial y} + \frac{\partial A_z^T}{\partial v}\frac{\partial v}{\partial y}\right)^2\Bigg] dxdy \end{aligned} \tag{4.16a}$$

$$W_m = \frac{1}{2}\int_{-\infty}^{+\infty}\int_{-\infty}^{+\infty}\frac{1}{\mu}\left[\left(\frac{\partial A_z^T}{\partial u}\frac{\partial u}{\partial x}\right)^2 + \left(\frac{\partial A_z^T}{\partial v}\frac{\partial v}{\partial x}\right)^2 + \left(\frac{\partial A_z^T}{\partial u}\frac{\partial u}{\partial y}\right)^2 + \left(\frac{\partial A_z^T}{\partial v}\frac{\partial v}{\partial y}\right)^2\right] dxdy \tag{4.16b}$$

Incorporating Equation (A.1) and (A.2) in (4.16b) yields:

$$W_m = \frac{1}{2}\int_{-\infty}^{+\infty}\int_{-\infty}^{+\infty}\frac{M^2}{\mu}\left[\left(\frac{\partial A_z^T}{\partial u}\right)^2 + \left(\frac{\partial A_z^T}{\partial v}\right)^2\right] dxdy \tag{4.17}$$

Finally, the magnetic energy stored in a unit length of the mapped domain can be calculated by changing the integration variables of Equation (4.17), which can be achieved using the rule expressed in Equation (4.11):

$$W_m = \frac{1}{2}\iint_{S^T}\frac{1}{\mu^T}\left[\left(\frac{\partial A_z^T}{\partial u}\right)^2 + \left(\frac{\partial A_z^T}{\partial v}\right)^2\right] dudv \tag{4.18}$$

From Equation (4.18), it can be observed that the mapping factor does not appear in the calculation of the magnetic energy in the mapped space, which means that it remains unchanged under conformal mapping.

The magnetic energy is related to the inductance matrix ($\mathbf{L}$) by [55]:

$$W_m = \frac{1}{2}\mathbf{I}^{t*}\mathbf{L}\mathbf{I} \tag{4.19}$$

where $\mathbf{I}$ is the $N \times 1$ vector representing the line current, N is the number of conductors and $t*$ represents the complex conjugate transpose.

In the original space, the elements of the current vector can be obtained by the calculation of the surface integration of the total current density over the cross section of the conductors ($J_{z_i}^{tot}$). So, the current in the i^{th} conductor is calculated by:

$$I_i = \iint_{S_{c_i}} J_{z_i}^{tot} dxdy \tag{4.20}$$

The total current density can be written as a composition of two others, one related to an arbitrary external current that is imposed on the conductor and the other given by the eddy current [32]. So, the total current density in the i^{th} conductor ($i = 1, \cdots, N$) can be expressed as:

$$J_i^{tot} = J_i^{ex} + J_i^{ed} = \sigma \mathbf{E} \tag{4.21}$$

Considering Equation (3.2a) and recalling that only the z component of the current is relevant to this study yields:

$$J_{z_i}^{tot} = \sigma \Delta V - j\omega\sigma A_z \tag{4.22}$$

Then, the total current density in the i^{th} conductor in the original and mapped space can be given as:

$$\begin{aligned} J_{z_i}^{tot} &= J_{z_i}^{ex} - j\omega\sigma A_z \\ &= J_{z_i}^{Tex} - j\omega\sigma^T A_z^T \\ &= J_{z_i}^{Ttot} \end{aligned} \tag{4.23}$$

The current in the original space calculated in the mapped space can be obtained by changing variables from Equation (4.20) resulting in:

$$I_i = \iint_{S_{c_i}^T} \frac{J_{z_i}^{Ttot}}{M^2} du dv \tag{4.24}$$

Finally, the elements of the inductance matrix can be calculated by equating (4.18) and (4.19) at each frequency, resulting in a set of K linearly-independent equations and K unknowns. Because of reciprocity (*i.e.*, $l_{ij} = l_{ji}$), the number of equations and the number of unknowns can be determined by:

$$K = \frac{N(N+1)}{2} \tag{4.25}$$

4.1.2 Resistance Matrix

The per-unit-length resistance matrix **R** is determined using the dissipated electric energy (resistive loss) due to the longitudinal component of the electric field obtained from the solution of the quasi-stationary problem. The resistive loss dissipated in a unit length of the unbounded domain (original space) can be calculated by:

$$\begin{aligned} W_R &= \int_{-\infty}^{+\infty}\int_{-\infty}^{+\infty} \sigma |\mathbf{E}|^2 dxdy \\ &= \int_{-\infty}^{+\infty}\int_{-\infty}^{+\infty} \sigma E_z^2 dxdy \end{aligned} \tag{4.26}$$

The dissipated energy in the mapped space can be calculated following a similar procedure to that used for the calculation of the magnetic energy in the mapped space: substituting electric field components by their corresponding values in terms of V and A_z, and changing integration variables. Following this process results in:

$$W_R = \iint_{S^T} \sigma^T (\Delta V^{T^2} + \omega^2 |A_z^T|^2) \frac{1}{M^2} dudv \tag{4.27}$$

The dissipated electric energy is related to the resistance matrix (**R**) by [55]:

$$W_R = \mathbf{I}^{t*}\mathbf{R}\mathbf{I} \tag{4.28}$$

The elements of the resistance matrix can be obtained by equating (4.27) and (4.28), which again will result in a set of K linearly-independent equations and K unknowns, where K is given by Equation (4.25).

4.2 Shunt Admittance of the Line

According to what was mentioned in Section 2.1.2, the transverse or shunt admittance is composed of two components, a conductance and a capacitance. However, the effect of the shunt conductance is assumed to be very small, therefore it can be neglected. For that reason, this section will describe a procedure for extracting the Capacitance Matrix (**C**) of an arbitrary transmission line.

4.2.1 Capacitance Matrix

The electric field energy method will be used for the calculation of the self and mutual capacitance of the transmission line. The electric energy stored in a unit length of the unbounded domain (original space) can be calculated by [49]:

$$W_e = \frac{1}{2}\int_{-\infty}^{+\infty}\int_{-\infty}^{+\infty} \varepsilon |\mathbf{E}|^2 dxdy \tag{4.29}$$

From the electrostatic approximation and substituting Equation (3.2a) in (4.29) results in:

$$W_e = \frac{1}{2}\int_{-\infty}^{+\infty}\int_{-\infty}^{+\infty} \varepsilon (-\nabla V)^2 dxdy \tag{4.30a}$$

$$W_e = \frac{1}{2}\int_{-\infty}^{+\infty}\int_{-\infty}^{+\infty} \varepsilon \left[\left(\frac{\partial V}{\partial x}\right)^2 + \left(\frac{\partial V}{\partial y}\right)^2\right] dxdy \tag{4.30b}$$

Now, applying the chain rule to Equation (4.30b) and then considering Equation (A.3a) results in:

$$\begin{aligned} W_e = \frac{1}{2}\int_{-\infty}^{+\infty}\int_{-\infty}^{+\infty} \varepsilon \Bigg[&\left(\frac{\partial V^T}{\partial u}\frac{\partial u}{\partial x} + \frac{\partial V^T}{\partial v}\frac{\partial v}{\partial x}\right)^2 \\ &+ \left(\frac{\partial V^T}{\partial u}\frac{\partial u}{\partial y} + \frac{\partial V^T}{\partial v}\frac{\partial v}{\partial y}\right)^2\Bigg] dxdy \end{aligned} \tag{4.31a}$$

$$W_e = \frac{1}{2}\int_{-\infty}^{+\infty}\int_{-\infty}^{+\infty}\varepsilon\left[\left(\frac{\partial V^T}{\partial u}\frac{\partial u}{\partial x}\right)^2 + \left(\frac{\partial V^T}{\partial v}\frac{\partial v}{\partial x}\right)^2 + \left(\frac{\partial V^T}{\partial u}\frac{\partial u}{\partial y}\right)^2 + \left(\frac{\partial V^T}{\partial v}\frac{\partial v}{\partial y}\right)^2\right]dxdy \tag{4.31b}$$

Incorporating Equations (A.1) and (A.2) in (4.31b) yields:

$$W_e = \frac{1}{2}\int_{-\infty}^{+\infty}\int_{-\infty}^{+\infty}\varepsilon M^2\left[\left(\frac{\partial V^T}{\partial u}\right)^2 + \left(\frac{\partial V^T}{\partial v}\right)^2\right]dxdy \tag{4.32}$$

Finally, the electric energy stored in a unit length of the mapped domain can be calculated by changing the integration variables of Equation (4.32), which can be achieved using the rule expressed in Equation (4.11):

$$W_e = \frac{1}{2}\iint_{S^T}\varepsilon^T\left[\left(\frac{\partial V^T}{\partial u}\right)^2 + \left(\frac{\partial V^T}{\partial v}\right)^2\right]dudv \tag{4.33}$$

It can be observed, from Equation (4.33), that the mapping factor does not appear in the calculation of the electric energy in the mapped space, which means that it remains unchanged under conformal mapping.

The electric energy is related to the capacitance matrix ($\mathbf{C}$) by [55]:

$$W_e = \frac{1}{2}\mathbf{V}^{t*}\mathbf{C}\mathbf{V} \tag{4.34}$$

where $\mathbf{V}$ is the $N \times 1$ vector representing the line voltage, N is the number of conductors and $t*$ represents the complex conjugate transpose. The line voltage is in fact the external excitation electric potential in the quasi-electric problem.

The elements of the capacitance matrix can be obtained by equating (4.33) and (4.34), which again will result in a set of K linearly-independent equations and K unknowns, where K is given by Equation (4.25).

4.3 Summary

In this chapter, the basic assumptions for calculating the parameters of an arbitrary transmission line, including overhead line and underground cable, are discussed. The main equations are derived from Maxwell's equations, which are solved with the finite element method after transforming the unbounded space into two unit circles through a conformal mapping technique. After finding a solution for the governing equations in the mapped space, the power loss, the magnetic energy and the electric energy are calculated in order to obtain the resistances, inductances and capacitances, respectively. Next chapter will present some study cases and the results after applying the method proposed in this chapter.

Chapter 5

Results and Discussion

In this chapter, the approach described in Chapter 4 is employed to determine the frequency-dependent per-unit-length series impedance and shunt admittance of overhead transmission lines and underground cables. In the study cases, the earth is considered to be a homogeneous lossy medium. Nevertheless, nothing prevents this technique to be applied to multi-layer, stratified models of the earth. Another assumption is that the sag of the overhead lines is not considered, since the approach is for a two-dimensional model of the transmission line.

As mentioned before, the solution of Equations (4.4) and (4.6) are obtained using the AC/DC Module of COMSOL Multiphysics to simulate electric and magnetic fields. The analytical results are obtained using PSCAD™/EMTDC™, which can represent the ground return impedance for overhead lines either by direct numerical integration of Carsons integral or by Deri's approximation, and for underground cables it gives the option to choose between direct numerical integration of Pollaczeks integral or Wedepohl's approximation.

As mentioned in Section 3.3, the interface between the upper and lower spaces ($y = 0$) is mapped to the boundaries of the mapped circles, and the boundary of the upper circle ($v > 0$) is paired with the boundary of the lower circle ($v < 0$) and a continuity boundary condition is applied on both of them. Consequently, the magnetic and electric scalar potentials (A_z^T and V_T) on the

boundary of the upper circle is symmetrically the same as that on the lower circle. In other words, applying these conditions to the boundaries of the circles is preserving the continuity between the upper and lower circles, even though they are graphically separated. The concept of this continuity will be better understood as illustrated in Fig. 5.1 and Fig. 5.2.

Some of the transmission line cases (including overhead line and underground cable) simulated and analyzed during the research will be described in the following sections.

5.1 Two Identical Parallel Conductors in Free Space

The first analyzed case consists of two parallel, perfectly conducting wires in free space. The radius (r_c) of each conductor is 2 cm and the separation distance (d) between the centres of both conductors is 1 m.

The analytical equation for the per-unit-length inductance of parallel wires in free space is given by:

$$\begin{aligned} l &= \frac{\mu_0}{\pi} \ln\left(\frac{d}{r_c}\right) \\ &= \frac{4\pi \times 10^{-7}}{\pi} \ln\left(\frac{1}{0.02}\right) \\ &= 1.5648 \text{ µH/m} \end{aligned} \tag{5.1}$$

And the analytical equation for the per-unit-length capacitance of parallel wires in free space is given by:

$$\begin{aligned} c &= \frac{\pi\varepsilon_0}{\ln\left(\frac{d}{2r_c} + \sqrt{\frac{d^2}{4r_c^2} - 1}\right)} \\ &= 7.1112 \text{ pF/m} \end{aligned} \tag{5.2}$$

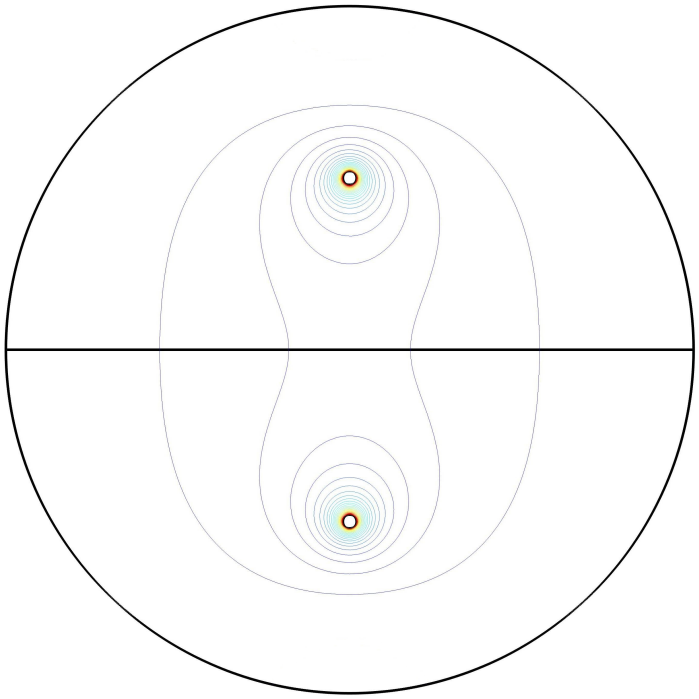

Fig. 5.1: Magnetic flux density contours for two parallel wires in free space in the original space.

Fig. 5.1 shows the two parallel conductors in the original space considering a truncation of 1 m (different truncation radii were used for the calculation of the parameters). Fig. 5.2 shows the unbounded region with the parallel conductors mapped into the circles using the proposed mapping scheme. For the sake of illustration to help understand how the field distribution varies in the mapped space, the magnetic flux density is plotted in the original and mapped space. The conductors are located at $x = 0$ and $y = \pm 0.5$ m, and as expected, in the mapped domain, each conductor is located inside a different circle. Note that the cross section of each mapped wire is still a circle (but different in size and location). Applying a magnetic insulation condition on the

boundary of the truncation case results in an electric current on the boundary that is not real causing an error in the calculation of the currents in the conductors. In order to avoid this error, a zero-current boundary condition ($J_z = 0$) is applied on the outer boundary of the truncation. The same zero-current boundary condition is applied in the mapped case, in addition, the boundaries are paired by a continuity boundary condition. These boundary conditions in both cases (truncated and mapped) will be applied in all examples that are presented in this chapter.

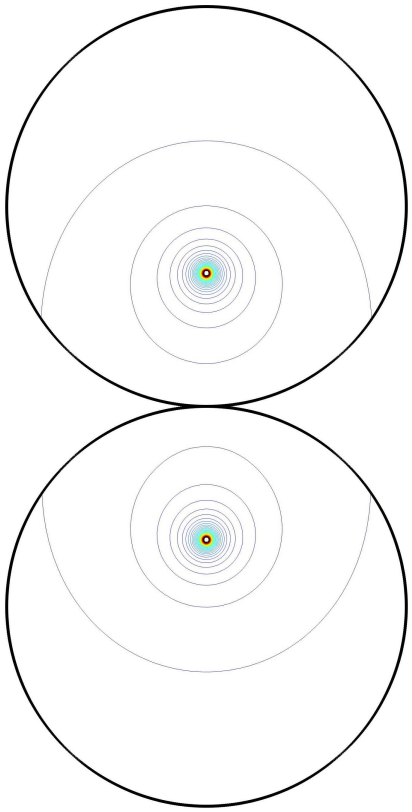

Fig. 5.2: Magnetic flux density contours for two parallel wires in free space in the mapped space.

Before proceeding to the calculation of the parameters, it will be proved that the magnetic potential remains the same in the original and mapped spaces, as stated in Equation (4.7a). For that purpose, A_z will be calculated at some points in a vertical line between the origin and the conductor in the original space (with a truncation radius of 50 m) and in the corresponding points of the mapped space, as given in Table 5.1. The values of v in terms of y, considering that $x = 0$, can be calculated by modifying Equation (3.19b) to:

$$v = \frac{2y}{1 + |y|} \tag{5.3}$$

Table 5.1: Comparison of the magnetic potential between the original and mapped spaces.

y [m]	v [m]	$\lvert A_z \rvert$ [Wb/m]	$\lvert A_z^T \rvert$ [Wb/m]
0	0	1.64469×10^{-8}	3.12756×10^{-8}
0.025	0.04878	0.02561	0.02557
0.05	0.09524	0.05134	0.0513
0.075	0.13953	0.07734	0.07728
0.1	0.18182	0.10374	0.10367
0.125	0.22222	0.13069	0.13061
0.15	0.26087	0.15838	0.15828
0.175	0.29787	0.18701	0.18688
0.2	0.33333	0.2168	0.21665
0.225	0.36735	0.24805	0.24787
0.25	0.4	0.28112	0.28092
0.275	0.43137	0.31649	0.31625
0.3	0.46154	0.35478	0.35449
0.325	0.49057	0.39686	0.39652
0.35	0.51852	0.444	0.44358
0.375	0.54545	0.49816	0.49765
0.4	0.57143	0.56262	0.56196
0.425	0.59649	0.64351	0.64261
0.45	0.62069	0.75468	0.7533
0.475	0.64407	0.94062	0.93781

The magnetic potential calculated in the mapped space is very approximate to that obtained in the original space. This difference is due to the truncation in the original space and to the number

of meshes used in each case. The result from Table 5.1 is shown in Fig. 5.3 as a function of the coordinate of the original space (y).

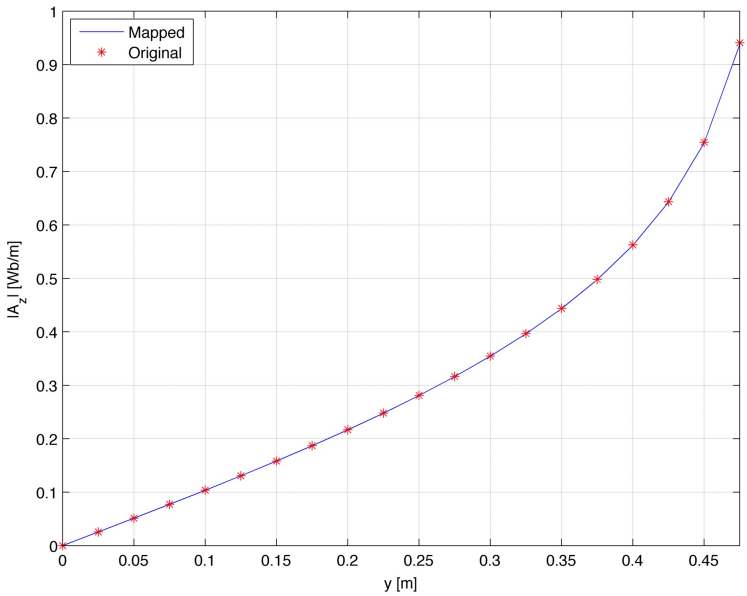

Fig. 5.3: Comparison of the magnetic potential calculated in both spaces.

The per-unit-length inductance will be calculated by simulating using the truncation method (with different truncation radii: 1, 5, 10 and 20 m) and the mapping scheme. This will be possible by calculating the magnetic energy given by Equation (4.15) for the original space, and Equation (4.18) for the mapped space, and then using circuit relation for inductance, as given in Equation (4.19). Equivalently, the electric energy will be determined using Equation (4.30b) for the original space and Equation (4.33) for the mapped space, and then in combination with Equation (4.34) result in the per-unit-length capacitance.

Table 5.2: Per-unit-length inductance and capacitance of two parallel-wires calculated with the analytical equations, the proposed mapping method and the truncation of the original space method.

	Analytical	Mapping	Truncation [m]			
			1	5	10	20
Inductance [µH/m]	1.5648	1.5711	1.7945	1.6553	1.6417	1.6362
Capacitance [pF/m]	7.1112	7.1106	6.2921	7.0757	7.1027	7.1098
Number of Meshes	-	2678	2418	2652	2601	2837

Table 5.2 shows these results in comparison with the analytical solution given in Equation (5.1) for the inductance and Equation (5.2) for the capacitance. The following table shows how many meshes the truncation method would need in order to obtain a similar result from the proposed mapping method.

Table 5.3: Comparison of the number of meshes and computational time of the per-unit-length inductance of two parallel-wires calculated for the proposed mapping method and the truncation of the original space method.

	Mapping	Truncation [m]				
		1	5	10	20	50
Inductance [µH/m]	1.5711	1.7686	1.5731	1.5736	1.5722	1.5730
Number of Meshes	2678	3432415	1119151	296775	77627	22555
Computational Time [s]	3	105	29	8	5	3

As observed in Table 5.2, the mapping method yields results very close to those obtained from analytical formulation for both cases, inductance and capacitance, whereas the truncation method gives accurate results only when the truncation radius becomes large, or as seen in Table 5.3 when the number of meshes inscreases considerably, which requires more memory, significant processing effort, and increased computation time. The case of 1 m of truncation was not able to approach the expected result even after achieving more than three million meshes.

5.2 Overhead Transmission Line over Lossy Ground

In the following cases, the ground is considered in the simulation and it is assumed to be a homogeneous lossy medium. In the original space, the x axis determines the air-ground interface. In the mapped space, the lower circle represents the ground and the upper circle represents the air in which the conductor(s) will be located.

5.2.1 One Conductor over Lossy Ground

For this study case, in terms of the original space, the ground ($\sigma_g = 0.01$ S/m and $\varepsilon_{r_g} = 4$) is located at $y < 0$ and the air ($\sigma_{air} = 0$ S/m and $\varepsilon_{r_{air}} = 1$) is located at $y > 0$. A single conductor made of copper ($\sigma_c = 5.998 \times 10^7$ S/m) with a circular cross section of 2 cm of radius (r_c) is located in the air at $x = 0$ and $y = 0.5$ m.

Similar to the previous example, the per-unit-length resistance and inductance are calculated as a function of frequency using the analytical formulation given in Chapter 2, the proposed mapping method and the truncation method (with different truncation radii: 2, 5 and 20 m). The results are shown in Fig. 5.4, for the resistance, and Fig. 5.5, for the inductance.

Fig. 5.4 shows a very good consistency between the per-unit-length resistance calculated using PSCAD™/EMTDC™ (which uses Carson's approximation for the overhead transmission line) and the mapping method. The same can be observed in Fig. 5.5 for the per-unit-length inductance. In both cases, the differences between the analytical solution and the truncation method are noticeable from the low-frequency range up to higher frequencies depending on the truncation radius, *i.e.* the difference decreases as the truncation radius increases. As mentioned in Chapter 3, this problem arises because at low frequencies the skin depth of the ground becomes comparable or greater than the truncation radius. Opposed to what happens in the resistance case, the inductance grows as the frequency decreases to zero, this characteristic cannot be represented in the truncation method even for larger truncation radii.

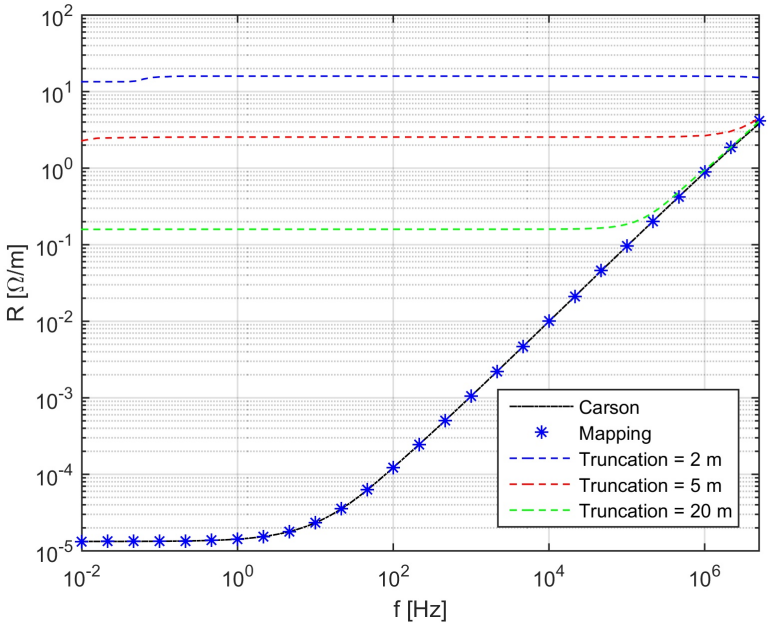

Fig. 5.4: PUL resistance for a single conductor over lossy ground versus frequency.

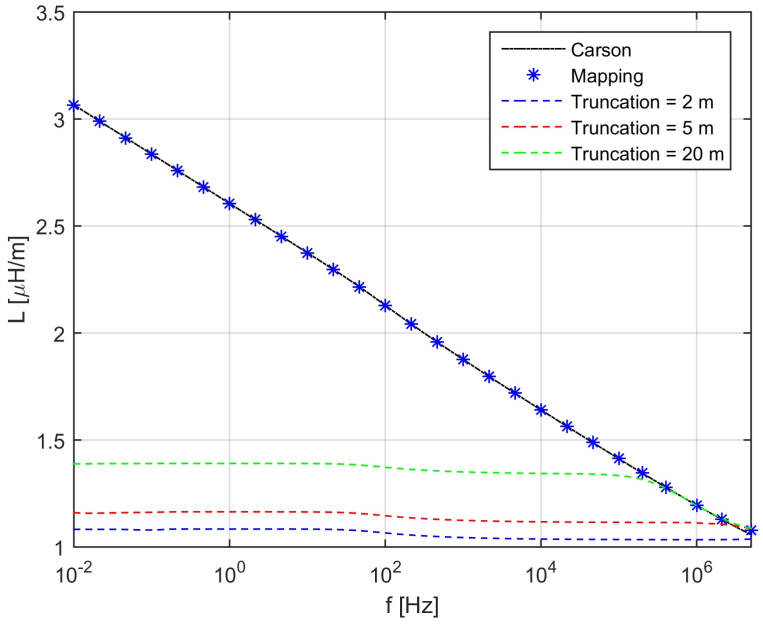

Fig. 5.5: PUL inductance for a single conductor over lossy ground versus frequency.

The method proposed in this thesis does not neglect the displacement current in the ground as in Carson's approximation. For this reason, a further inspection was performed to have a better understanding of the influence of the ground permittivity and conductivity on the per-unit-length inductance at the frequency range from 100 kHz to 5 MHz as observed in Fig. 5.6.

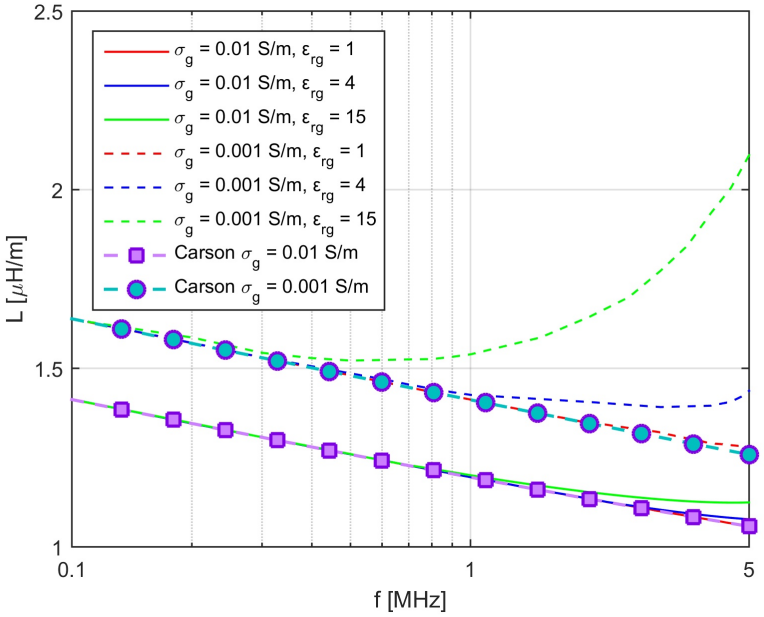

Fig. 5.6: PUL inductance for different values of ground conductivity and permittivity.

From Fig. 5.6 it is possible to observe that the inductance calculated with Carson's approximation loses accuracy as the frequency increases, so it becomes clear that neglecting the permittivity for the calculation of the parameters will lead to errors which are intensified as the ground permittivity increases and the ground conductivity decreases.

Just as for the resistance and inductance, the capacitance is determined using the proposed mapping and the truncation methods and then compared with the analytical result. These results are given in Table 5.4.

Fig. 5.7 shows the capacitance obtained from PSCAD™/EMTDC™ in comparison with the

Table 5.4: Per-unit-length capacitance of a single conductor over lossy ground obtained from the analytical solution, the proposed mapping method and the truncation of the original space method.

		Capacitance [pF/m]
Analytical		14.2209
Mapping		14.2222
Truncation [m]	1	12.5842
	5	14.1515
	10	14.2055
	20	14.2199

capacitance obtained with the mapping method, which is shown to be independent from the frequency.

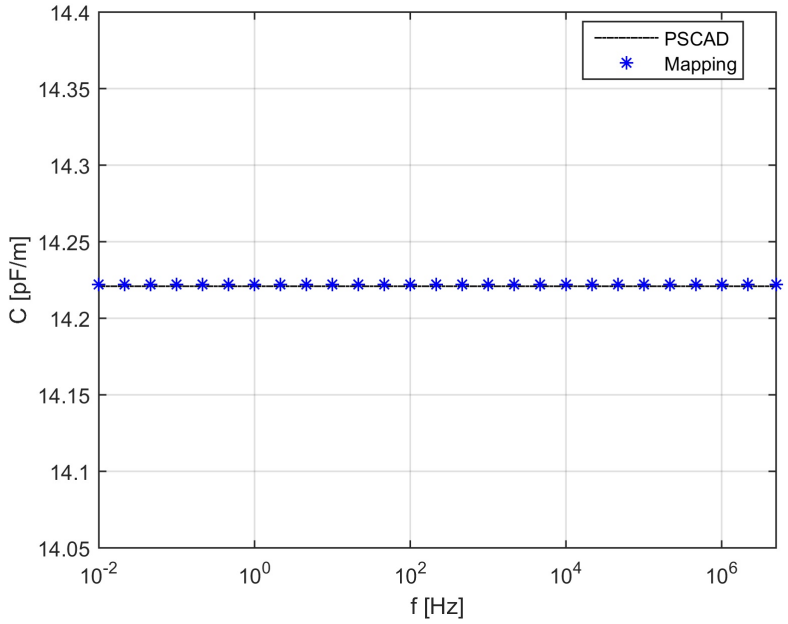

Fig. 5.7: PUL capacitance for a single conductor over lossy ground versus frequency.

Table 5.4 and Fig. 5.7 show that the mapping method yields results approximately the same to those obtained from analytical formulation for the per-unit-length capacitance. The trunca-

tion method gives accurate results only when the truncation becomes large, which reduces the performance of the simulation in terms of speed, memory and processing requirements.

As observed, the mapping method is able to provide accurate results in a wide range of frequencies for all three parameters: resistance, inductance and capacitance. Special attention should be given to the low-frequency range, where truncation methods fail to give an acceptable solution, and to the high-frequency range, where the permittivity of the ground cannot be neglected because the displacement current becomes comparable to the conduction current in the ground.

5.2.2 Two Conductors over Lossy Ground

From the previous example, it is possible to conclude that the truncation method does not give accurate solutions, for that reason it will be disregarded in the following study cases.

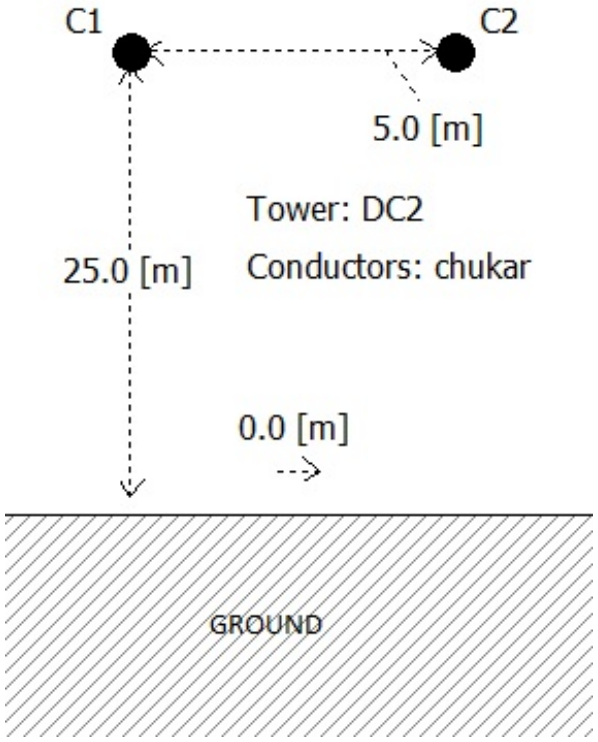

Fig. 5.8: Geometry of the two conductors over lossy ground.

In this case, two conductors over a lossy ground is simulated in COMSOL Multiphysics using the mapping method and then the results are compared with PSCAD™/EMTDC™. The same conductor and ground electrical parameters are used but with a different geometry. The radius (r_c) of each conductor is 2 cm and both conductors are located 25 m above the ground and are horizontally apart by 5 m as illustrated in Fig. 5.8.

Since there is more than one conductor now, the results will include the self and mutual parameters of the transmission line. Due to symmetry, the self resistances R_{11} and R_{22} and the mutual resistances R_{12} and R_{21} are the equal, the same happens to the inductances and capacitances. For this reason, only R_{11}, R_{12}, L_{11}, L_{12}, C_{11} and C_{12} are being plotted in the following figures.

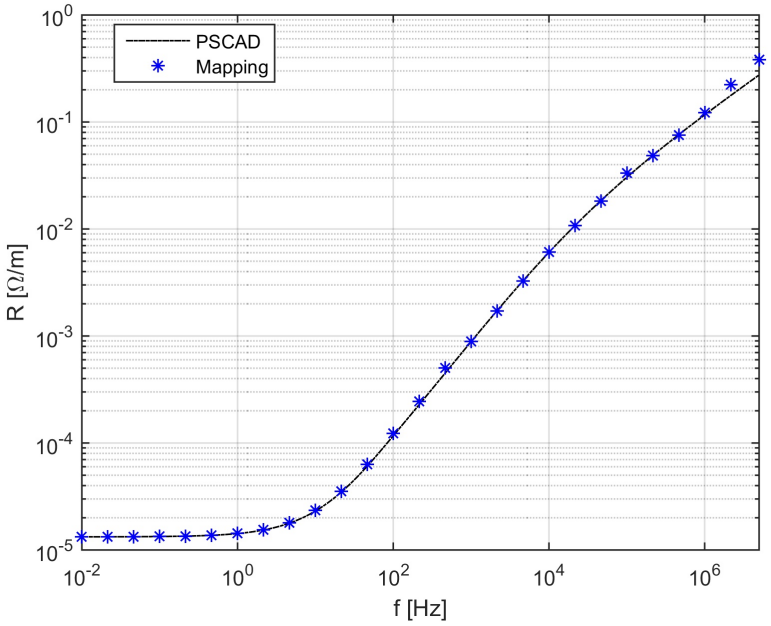

Fig. 5.9: PUL self resistance for two conductors over lossy ground versus frequency.

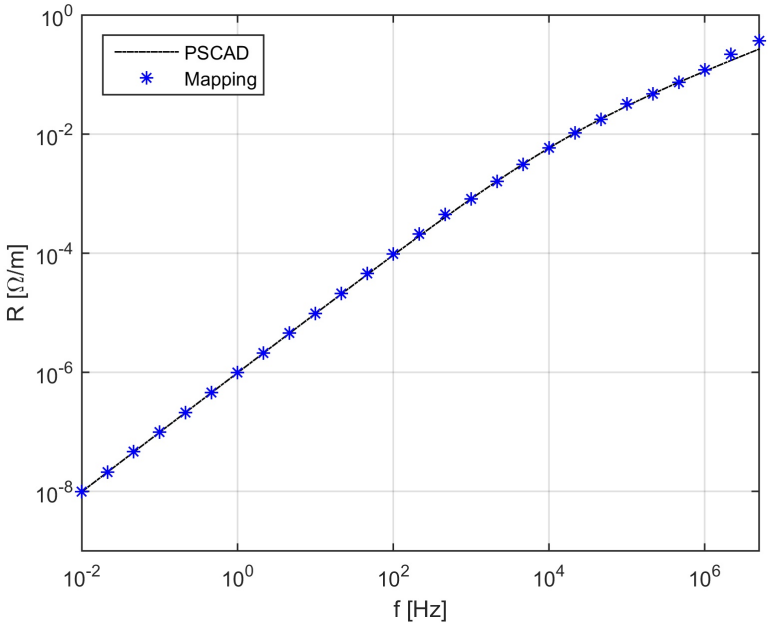

Fig. 5.10: PUL mutual resistance for two conductors over lossy ground versus frequency.

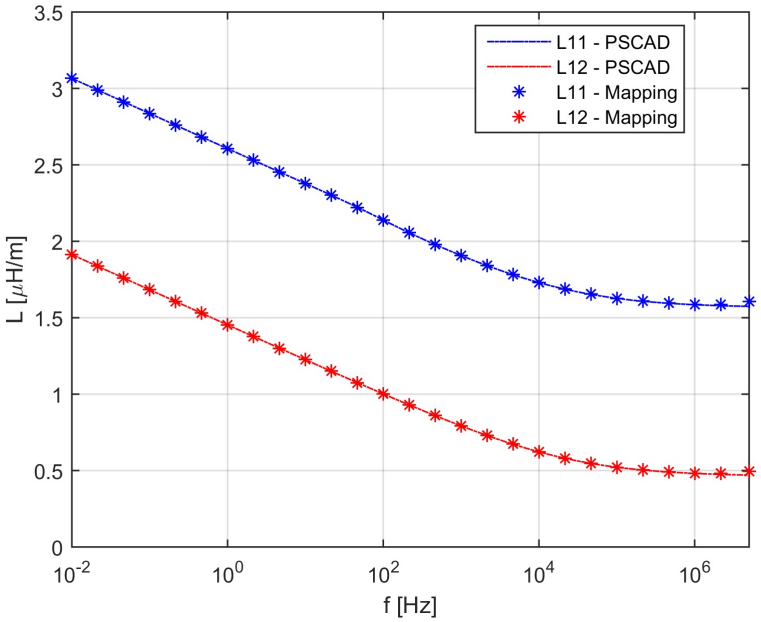

Fig. 5.11: PUL inductances for two conductors over lossy ground versus frequency.

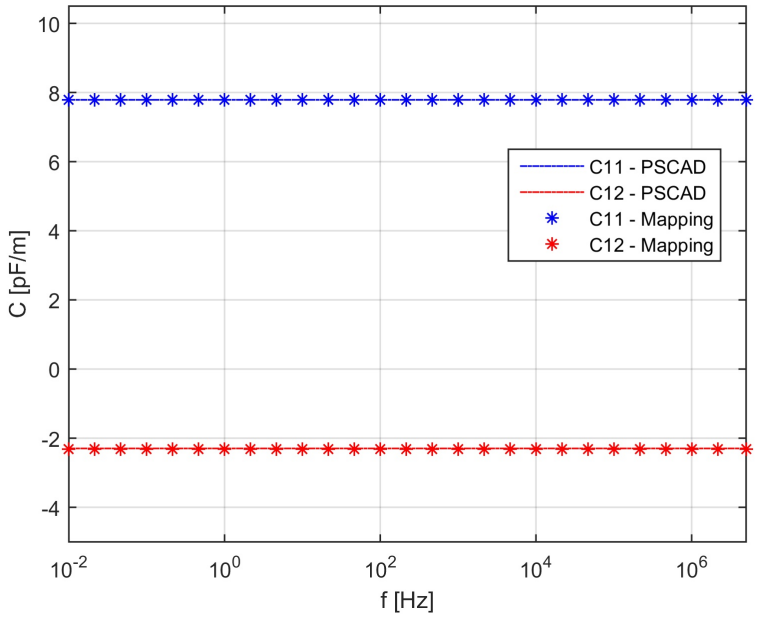

Fig. 5.12: PUL capacitances for two conductors over lossy ground versus frequency.

As observed in the figures above, the mapping method is able to provide accurate results in the full range of frequency under study for all three parameters: resistance, inductance and capacitance. Furthermore, the mapping method is able to describe, unlike the analytical formulations, the influence of the permittivity of the ground at higher frequencies.

5.2.3 Three Conductors over Lossy Ground

Up to now, all the examples studied were for verification purposes, but from now on more realistic cases will be considered. In this section, for example, a standard three phase transmission line obtained from PSCAD™/EMTDC™ will be studied.

The transmission line has three conductors with 2.035 cm of radius, a DC resistance of 0.03206 Ω/km, a flat horizontal separation between conductors of 9 m and located 12 m above the ground, as illustrated in Fig. 5.13.

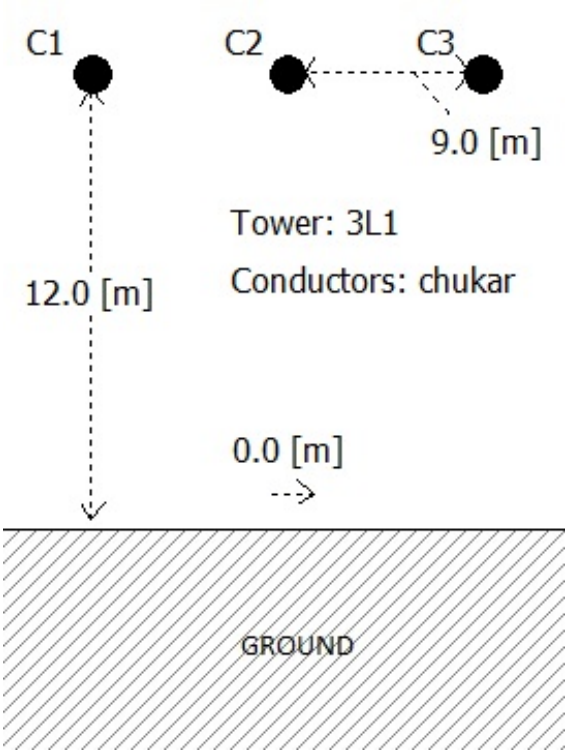

Fig. 5.13: Geometry of the three conductors over lossy ground.

The per-unit-length self and mutual resistances, inductances and capacitances for this transmission line are given in the following figures. Considering the symmetry of the geometry and that the distance between conductors is much higher than the conductors radii, some parameters will be equal, for this reason not all the parameters will be plotted in the following figures.

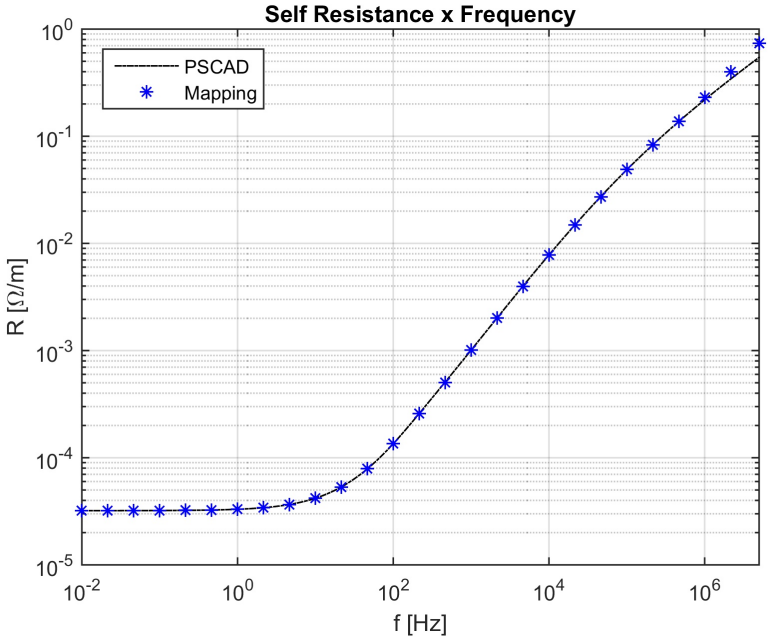

Fig. 5.14: PUL self resistance for three conductors over lossy ground versus frequency.

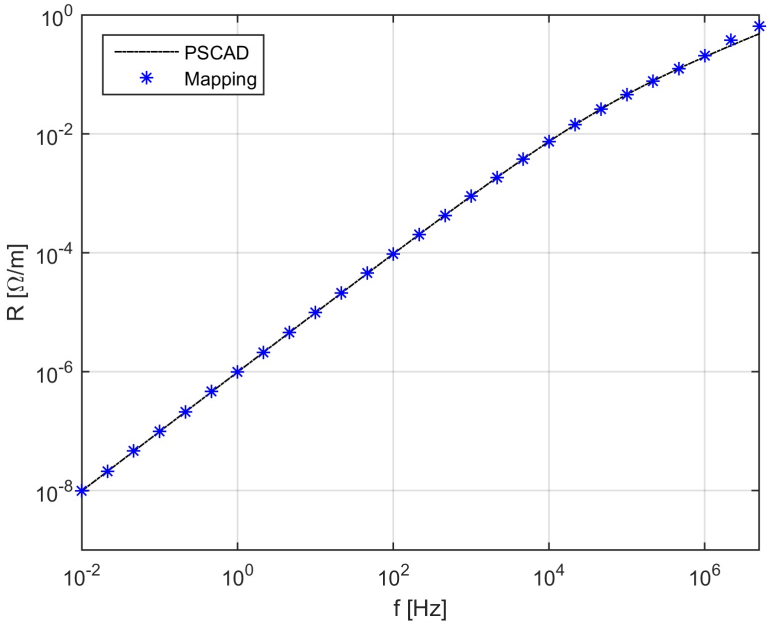

Fig. 5.15: PUL R_{12} for three conductors over lossy ground versus frequency.

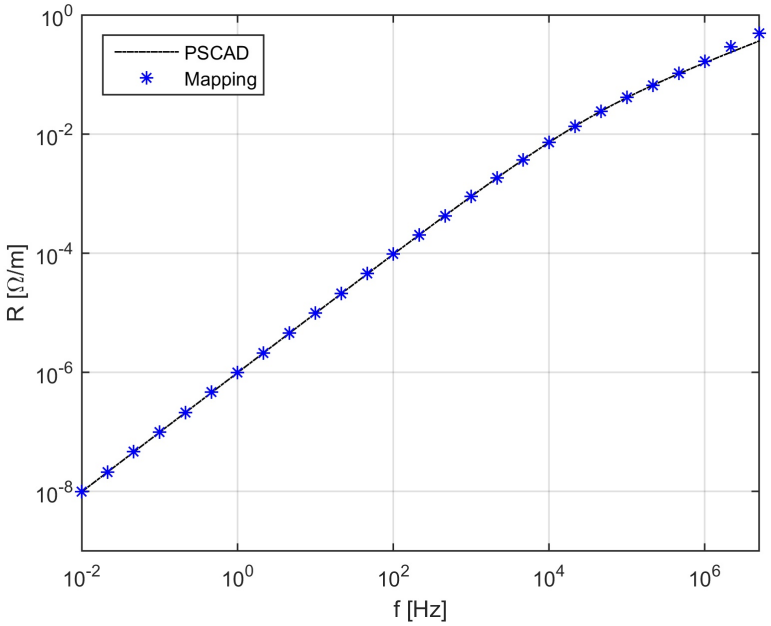

Fig. 5.16: PUL R_{13} for three conductors over lossy ground versus frequency.

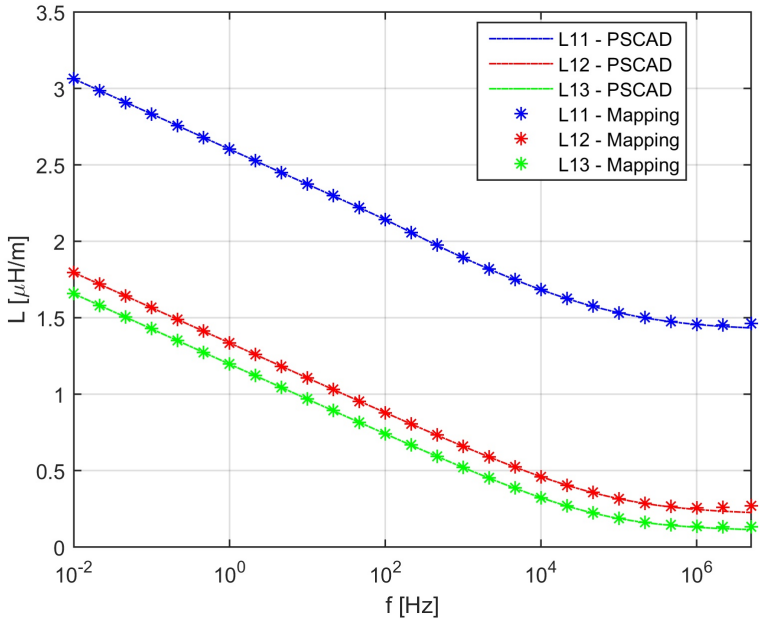

Fig. 5.17: PUL self and mutual inductances for three conductors over lossy ground versus frequency.

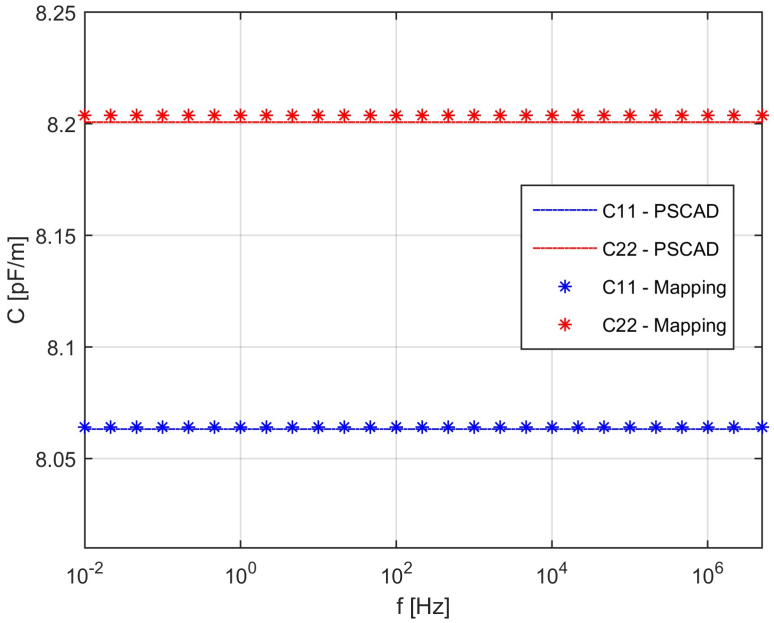

Fig. 5.18: PUL self capacitances for three conductors over lossy ground versus frequency.

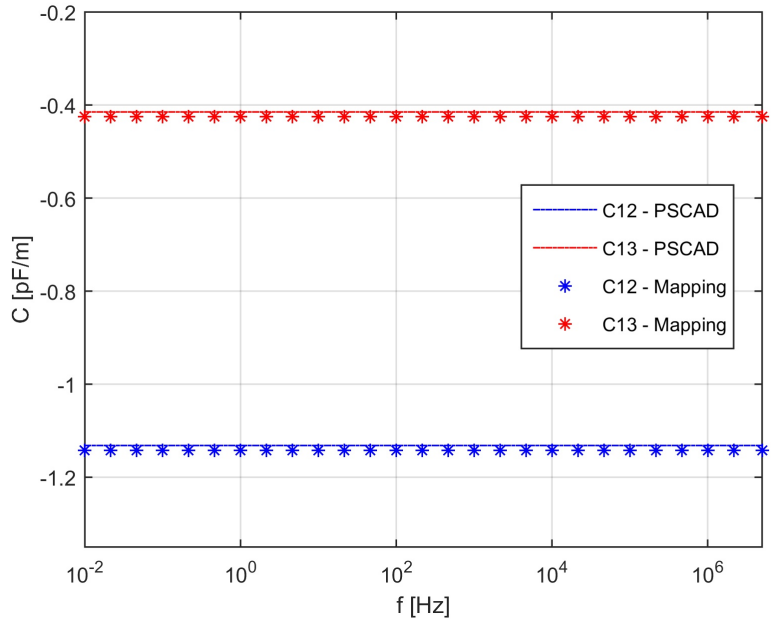

Fig. 5.19: PUL mutual capacitances for three conductors over lossy ground versus frequency.

Once again, one can observe in the figures above that the proposed method is accurate over a wide range of frequencies, and as mentioned before, it is able to give results considering the displacement current in the ground.

5.3 Underground Cables

In the following cases, it will be shown that it is also possible to apply the mapping technique to underground cables such as the coaxial cable and then to the sector-shaped cable, for which there is no analytical solution available.

5.3.1 Coaxial Cables

In this case, a coaxial cable is placed 1 m below the surface of the ground, and its geometry is as shown in Fig. 5.20.

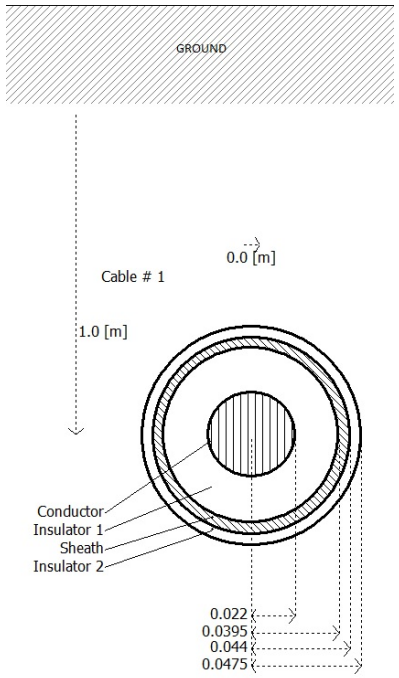

Fig. 5.20: Geometry of the coaxial cable.

The electric parameters such as conductivities and relative permittivities are as follows:

Conductivity of the core: $\sigma_c = 5.9524 \times 10^7$ S/m

Conductivity of the sheath: $\sigma_s = 4.5455 \times 10^6$ S/m

Conductivity of the ground: $\sigma_g = 0.01$ S/m

Relative permittivity of the inner dielectric insulator: $\varepsilon_{r_{id}} = 4.1$

Relative permittivity of the coating insulator: $\varepsilon_{r_{ci}} = 2.3$

Relative permittivity of the ground: $\varepsilon_{r_g} = 4$

Fig. 5.21 shows the coaxial cable in the mapped space (as expected, the coaxial cable remains circular but with different radii) that will be simulated in COMSOL Multiphysics, and then the per-unit-length self and mutual resistances, inductances and capacitances are compared with the results obtained from PSCAD™/EMTDC™ (which uses Wedepohl's approximation for the underground cables) as can be observed in Figs. 5.22-5.24.

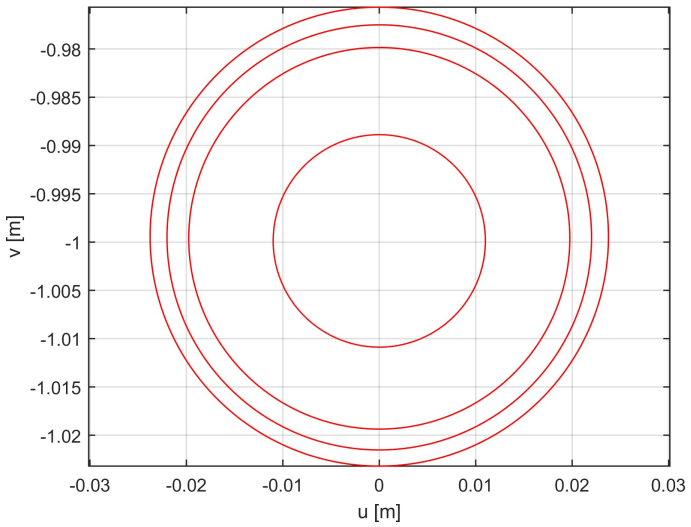

Fig. 5.21: Coaxial cable in the mapped space.

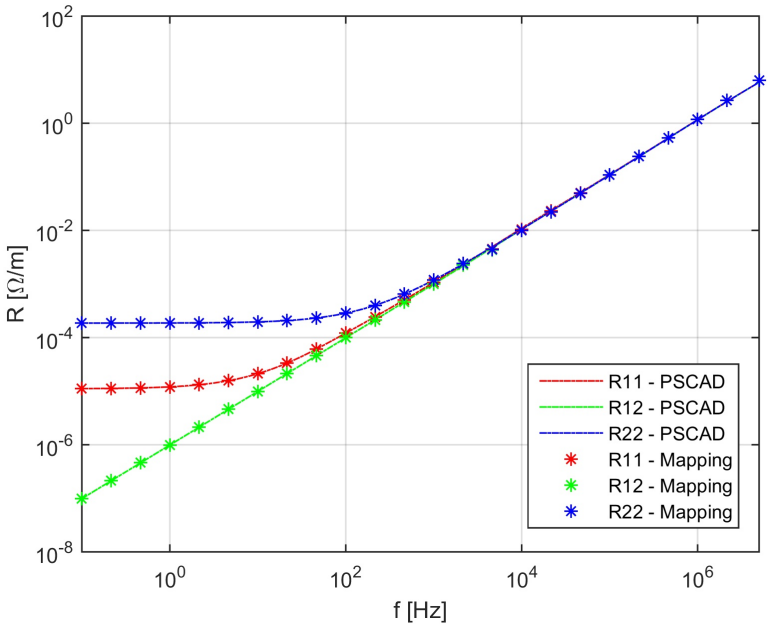

Fig. 5.22: PUL resistances for the coaxial cable versus frequency.

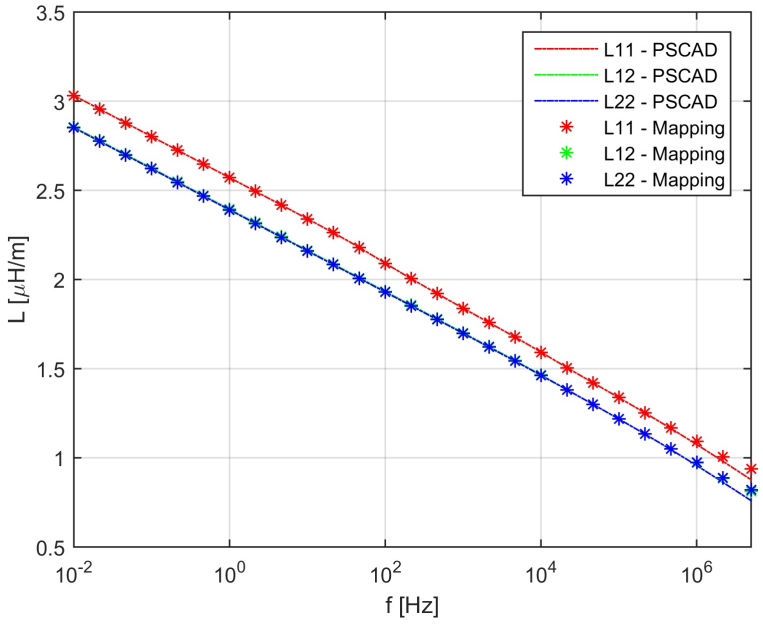

Fig. 5.23: PUL inductances for the coaxial cable versus frequency.

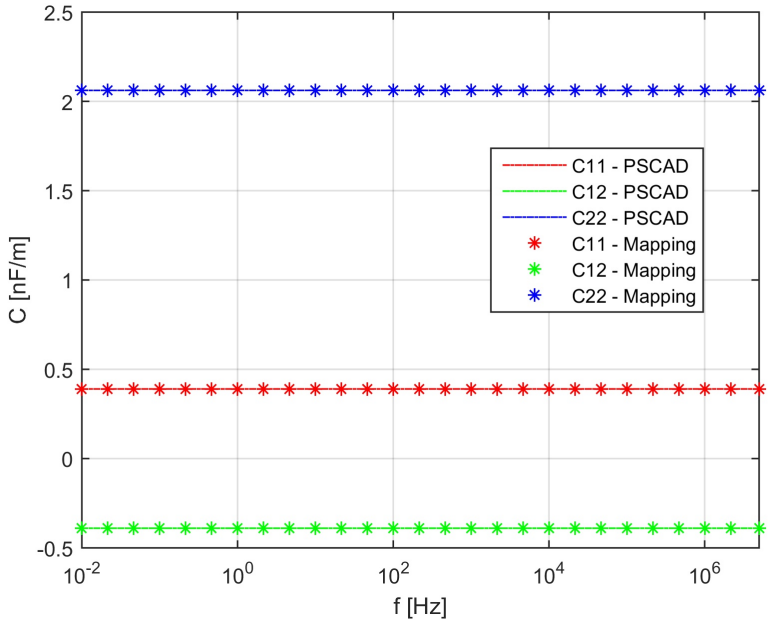

Fig. 5.24: PUL capacitances for the coaxial cable versus frequency.

From the figures above, it is possible to conclude that the proposed mapping method is also able to provide accurate results for all the parameters of an underground cable such as the coaxial cable. In order to verify the influence of the ground permittivity on the parameters, a zoom will be applied on Fig. 5.22 and Fig. 5.23, which should present some differences, considering that the proposed method does not neglect the displacement current in the ground.

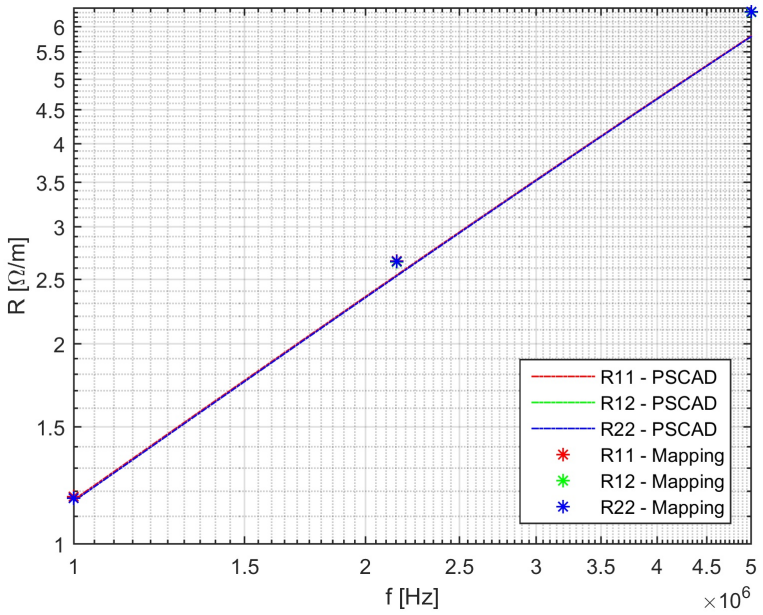

Fig. 5.25: Zoom of the PUL resistances for the coaxial cable versus frequency.

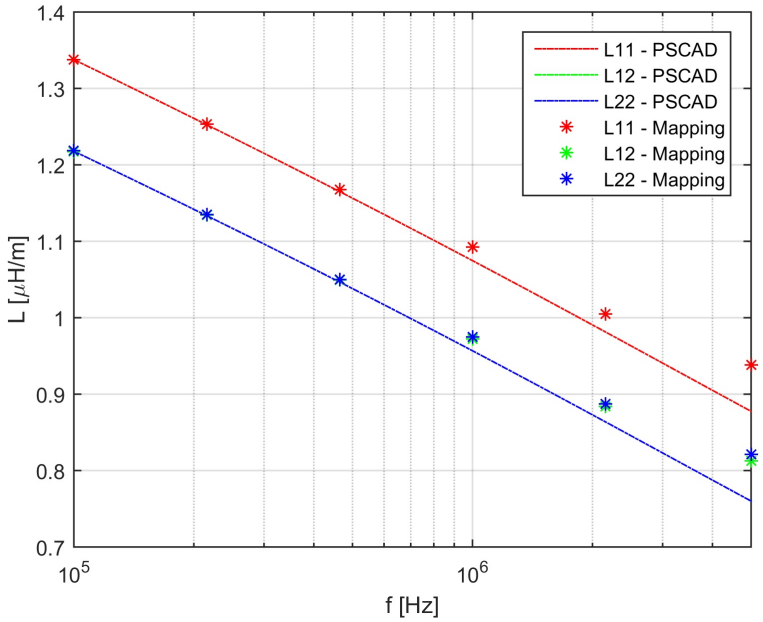

Fig. 5.26: Zoom of the PUL inductances for the coaxial cable versus frequency.

And, as observed in Fig. 5.25 and Fig. 5.26, the ground permittivity has a direct impact at the parameters at higher frequencies, in other words, neglecting the displacement current at the ground will yield inaccurate results.

5.3.2 Sector-Shaped Cable

The previous study cases demonstrate that the proposed method is able to calculate the parameters of any configuration commonly used for an overhead transmission line and underground cable. Those steps were important to demonstrate the accuracy of the proposed method before the calculation of the sector-shaped cable which, as mentioned before, has no analytical formulation available [3, 34, 44, 56, 57].

The dimensions and the electric parameters such as conductivities and relative permittivities for this study case are given in Fig. 5.27.

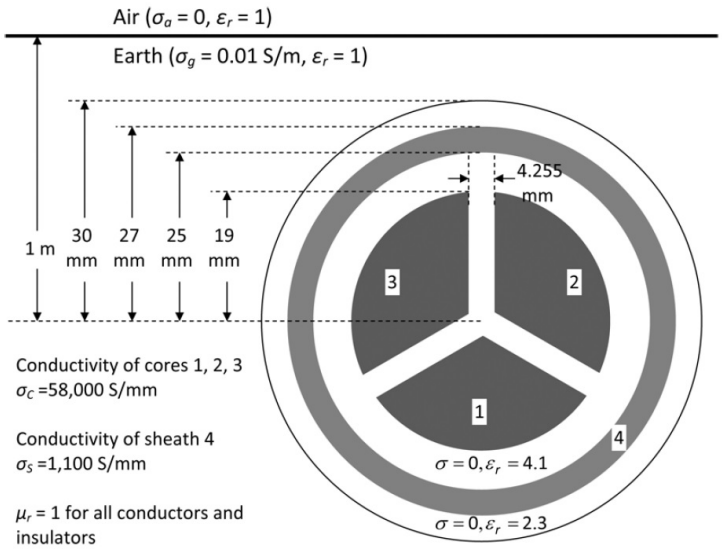

Fig. 5.27: Sector-shaped cable in the original space.

Fig. 5.28 shows the same sector-shaped cable in the mapped domain.

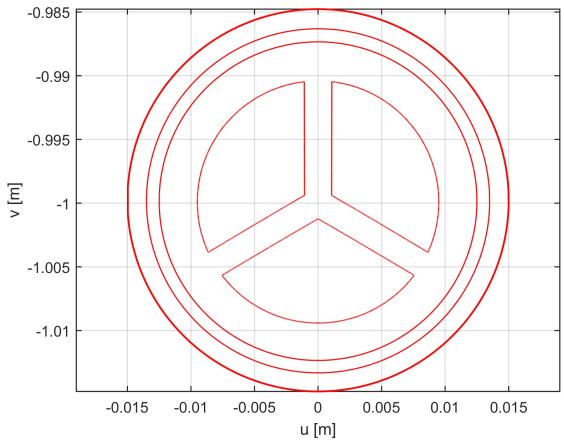

Fig. 5.28: Sector-shaped cable in the mapped space.

From Fig. 5.28, one may imply that a straight line in the original domain is transformed into another straight line in the mapped space, which is not true. They seem to be straight lines because the radius of the sector-shaped cable used in this example is very small. Just for the sake of illustration, Fig. 5.29 shows how the mapped sector-shapped cable would look like if the dimensions of the original cable were increased by a factor of thirty (30x).

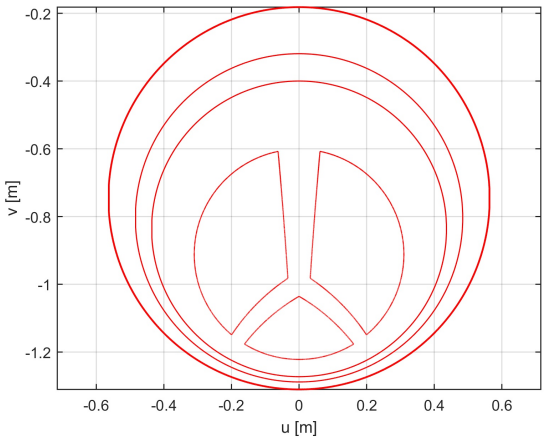

Fig. 5.29: Sector-shaped cable in the mapped space for increased dimensions.

The per-unit-length self and mutual resistances, inductances and capacitances for this sector-shaped cable are given in the following figures, since there is no analytical solution for this problem, this method could be used as reference for this geometry.

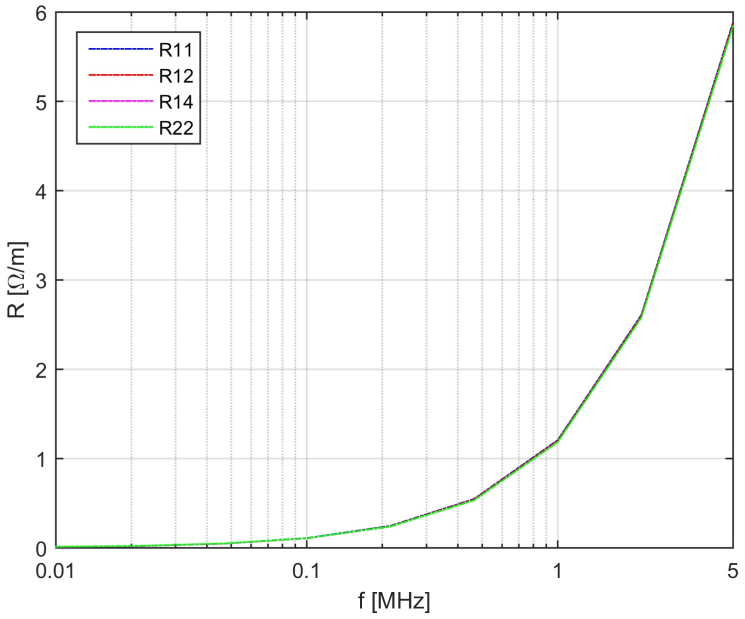

Fig. 5.30: PUL resistances for the sector-shaped cable versus frequency.

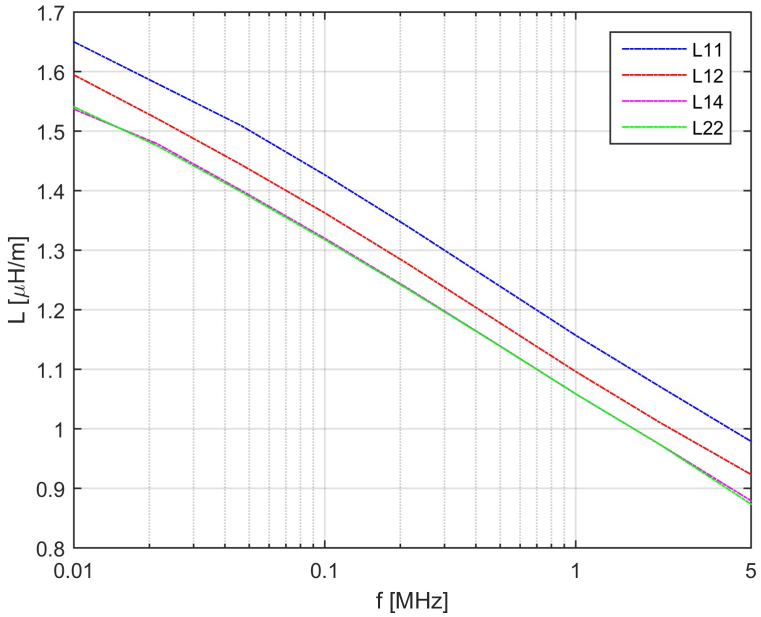

Fig. 5.31: PUL inductances for the sector-shaped cable versus frequency.

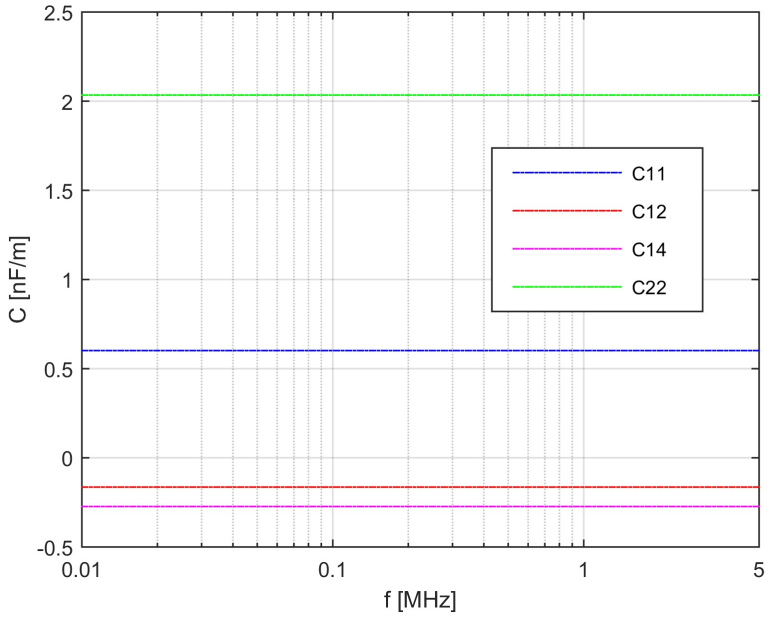

Fig. 5.32: PUL capacitances for the sector-shaped cable versus frequency.

Chapter 6

Conclusions and Recommendations

6.1 Conclusions and Summary of Work

In this thesis, a conformal spatial transformation together with the finite element method is presented for the determination of the per-unit-length parameter of a generic overhead transmission line or underground cable. The parameters that are more relevant for power system analysis are the series resistance and inductance and the shunt capacitance. The solution of the governing equations representing the two-dimensional quasi-stationary solution of the electric and magnetic fields were accomplished with the aid of COMSOL Multiphysics, a commonly used commercial finite element analysis software program.

The proposed mapping technique basically transforms the unbounded space into two unit circles, the upper one representing the air domain and the lower one representing the ground domain. The per-unit-length resistance and inductance were obtained by calculating the resistive losses and stored magnetic energy, respectively, both due to the longitudinal current in the conductor(s). The per-unit-length capacitance was calculated from the stored electric energy due to the in-plane current.

All these parameters were calculated for several overhead lines and underground cables, and

then compared with the analytical solution obtained from PSCAD™/EMTDC™ (which uses Carson's approximation and Wedepohl's formulation). Those steps were important to validate the proposed method for the calculation of the sector-shaped cable which unlike the other study cases, does not have an analytical formulation available. The proposed method provided better accuracy than the truncation method, showing that the conformal mapping approach is suitable to model unbounded spaces and arbitrary geometries without the need for a very large truncation boundary. This is a powerful resource, considering that it is more efficient and requires less computational memory and computation time.

The main objective of this research is to provide enough information to show that it is possible to use the proposed mapping technique to obtain the per-unit-length parameters of any generic overhead transmission line and underground cable, specially in those cases where there is no analytical solution for a given arbitrary geometry.

6.2 Recommendations for Future Research

Since the sector-shaped cable was the only case studied, which did not have an analytical solution, it would be interesting to study some other geometries with less standard shapes for future work. Furthermore, this method could also be applied to underwater cables.

Another recommendation is to develop an application to determine and export the mapped geometries for a given geometry in the original space to be used in COMSOL Multiphysics or any other FEM based simulation software program, this could make the drawing process easier and faster.

References

[1] W. D. Stevenson, *Elements of Power System Analysis*, 4th ed. New York: McGraw-Hill, 1982.

[2] C. R. Paul, *Analysis of Multiconductor Transmission Lines*, 2nd ed. Wiley-IEEE Press, 2008.

[3] Y. Yin, "Calculation of frequency dependent parameters of underground cables with finite element method," Ph.D. dissertation, University of British Columbia, 1990.

[4] M. M. I. Hashim, H. W. Ping, and V. K. Ramachandaramurthy, "Impedance-based fault location techniques for transmission lines," in *TENCON 2009 - 2009 IEEE Region 10 Conference*. IEEE, 2009, pp. 1–6.

[5] G. Sivanagaraju, S. Chakrabarti, and S. C. Srivastava, "Uncertainty in Transmission Line Parameters: Estimation and Impact on Line Current Differential Protection," *IEEE Transactions on Instrumentation and Measurement*, vol. 63, no. 6, pp. 1496–1504, 2014.

[6] A. R. Hileman, *Insulation Coordination for Power Systems*, 1st ed. New York: Marcel Dekker, Inc., 1999.

[7] J. R. Carson, "Wave Propagation in Overhead Wires with Ground Return," *Bell System Technical Journal*, vol. 5, no. 4, pp. 539–554, 1926.

[8] W. Sones and S. M. Wong, "Overview on transient overvoltages and insulation design for a high voltage transmission system," in *2010 International Conference on High Voltage Engineering and Application*. IEEE, 2010, pp. 12–17.

[9] E. C. M. Costa and S. Kurokawa, "Estimation of transmission line parameters using multiple methods," *IET Generation, Transmission & Distribution*, vol. 9, no. 16, pp. 2617–2624, 2015.

[10] R. Schulze, P. Schegner, and R. Zivanovic, "Parameter Identification of Unsymmetrical Transmission Lines Using Fault Records Obtained From Protective Relays," *IEEE Transactions on Power Delivery*, vol. 26, no. 2, pp. 1265–1272, 2011.

[11] M. Asprou and E. Kyriakides, "Estimation of transmission line parameters using PMU measurements," in *2015 IEEE Power & Energy Society General Meeting*, vol. 9. IEEE, 2015, pp. 1–5.

[12] L. Hofmann, "Series expansions for line series impedances considering different specific resistances, magnetic permeabilities, and dielectric permittivities of conductors, air, and ground," *IEEE Transactions on Power Delivery*, vol. 18, no. 2, pp. 564–570, 2003.

[13] R. A. Chipman, *Theory and Problems of Transmission Lines.* McGraw-Hill, 1968.

[14] O. M. O. Gatous, J. Pissolato, J. H. a. Monteiro, E. C. M. Costa, A. J. G. Pinto, and S. Kurokawa, "Simplified skin-effect formulation for power transmission lines," *IET Science, Measurement & Technology*, vol. 8, no. 2, pp. 47–53, 2014.

[15] F. Rachidi and S. Tkachenko, *Electromagnetic Field Interaction with Transmission Lines: From Classical Theory to HF Radiation Effects.* WIT Press, 2008.

[16] S. Bonyadi-ram, B. Kordi, and G. E. Bridges, "A full-space conformal mapping for the calculation of series impedance of overhead transmission lines and underground cables," *Electric Power Systems Research*, vol. 91, pp. 95–103, 2012.

[17] Qiushi Chen and A. Konrad, "A review of finite element open boundary techniques for static and quasi-static electromagnetic field problems," *IEEE Transactions on Magnetics*, vol. 33, no. 1, pp. 663–676, 1997.

[18] J. Imhoff, G. Meunier, X. Brunotte, and J. Sabonnadiere, "An original solution for unbounded electromagnetic 2D- and 3D-problems throughout the finite element method," *IEEE Transactions on Magnetics*, vol. 26, no. 5, pp. 1659–1661, 1990.

[19] Y. Saito, K. Takahashi, and S. Hayano, "Finite element solution of open boundary magnetic field problems," *IEEE Transactions on Magnetics*, vol. 23, no. 5, pp. 3569–3571, 1987.

[20] J.-M. Jin and D. Riley, "Finite Element Mesh Truncation," in *Finite Element Analysis of Antennas and Arrays.* Hoboken, NJ, USA: John Wiley & Sons, Inc., 2008, pp. 55–99.

[21] M. Ikeuchi, H. Sawami, and H. Niki, "Analysis of Open-Type Dielectric Waveguides by the Finite-Element Iterative Method," *IEEE Transactions on Microwave Theory and Techniques*, vol. 29, no. 3, pp. 234–240, 1981.

[22] P. Silvester, D. Lowther, C. Carpenter, and E. Wyatt, "Exterior finite elements for 2-dimensional field problems with open boundaries," *Proceedings of the Institution of Electrical Engineers*, vol. 124, no. 12, p. 1267, 1977.

[23] D. Lowther, C. Rajanathan, and P. Silvester, "A finite element technique for solving 2-D open boundary problems," *IEEE Transactions on Magnetics*, vol. 14, no. 5, pp. 467–469, 1978.

[24] C. Antunes, "Approximate ballooning techniques," *IEEE Transactions on Magnetics*, vol. 19, no. 6, pp. 2555–2557, 1983.

[25] G. Beer and J. L. Meek, "Infinite domain elements," *International Journal for Numerical Methods in Engineering*, vol. 17, no. 1, pp. 43–52, 1981.

[26] P. Bettess and J. A. Bettess, "Infinite elements for static problems," *Engineering Computations*, vol. 1, no. 1, pp. 4–16, 1984.

[27] M. McDougall and J. Webb, "Infinite elements for the analysis of open dielectric waveguides," *IEEE Transactions on Microwave Theory and Techniques*, vol. 37, no. 11, pp. 1724–1731, 1989.

[28] M. Towers, A. McCowen, and J. Macnab, "Electromagnetic scattering from an arbitrary, inhomogeneous 2-D object-a finite and infinite element solution," *IEEE Transactions on Antennas and Propagation*, vol. 41, no. 6, pp. 770–777, 1993.

[29] B. Nath and J. Jamshidi, "The w-plane finite element method for the solution of scalar field problems in two dimensions," *International Journal for Numerical Methods in Engineering*, vol. 15, no. 3, pp. 361–379, 1980.

[30] S. Wong and I. Ciric, "Method of Conformal Transformation for the Finite-Element Solution of Axisymmetric Exterior-Field Problems," *COMPEL - The international journal for computation and mathematics in electrical and electronic engineering*, vol. 4, no. 3, pp. 123–135, 1985.

[31] Ruey-Beei Wu and Chun Hsiuing Chen, "A Variational Analysis of Dielectric Waveguides by the Conformal Mapping Technique," *IEEE Transactions on Microwave Theory and Techniques*, vol. 33, no. 8, pp. 681–685, 1985.

[32] S. Cristina and M. Feliziani, "A finite element technique for multiconductor cable parameters calculation," *IEEE Transactions on Magnetics*, vol. 25, no. 4, pp. 2986–2988, 1989.

[33] S. Gomes Jr., C. Portela, and N. Martins, "Detailed Model of Long Transmission Lines for Modal Analysis of AC Networks," *International Conference on Power Systems Transients (IPST)*, no. June, pp. 1 – 6, 2001.

[34] R. A. Rivas, "Calculation of frequency-dependent parameters of power cables with digital images and partial subconductors," Ph.D. dissertation, University of British Columbia, 2001.

[35] H. B. Dwight, "Skin Effect in Tubular and Flat Conductors," *Transactions of the American Institute of Electrical Engineers*, vol. XXXVII, no. 2, pp. 1379–1403, 1918.

[36] D. E. Hedman, "Propagation on Overhead Transmission Lines II-Earth-Conduction Effects and Practical Results," *IEEE Transactions on Power Apparatus and Systems*, vol. 84, no. 3, pp. 205–211, 1965.

[37] M. Perz and M. Raghuveer, "Generalized Derivation of Fields, and Impedance Correction Factors of Lossy Transmission Lines Part I. Lossy conductors Above Lossless Ground," *IEEE Transactions on Power Apparatus and Systems*, vol. PAS-93, no. 6, pp. 1827–1831, 1974.

[38] F. Pollaczek, "Über das Feld einer Unendlich Langen Wechselstromdurchflossenen Einfachleitung," *Elektr. Nachr. Tech.*, vol. 3, pp. 339–359, 1926.

[39] H. Dommel, *Electromagnetic Transients Program: Reference Manual: (EMTP theory book)*. Bonneville Power Administration, 1986.

[40] M. Nakagawa, "Further Studies on Wave Propagatioin Along Overhead Transmission Lines: Effects of Admittance Correction," *IEEE Transactions on Power Apparatus and Systems*, vol. PAS-100, no. 7, pp. 3626–3633, 1981.

[41] A. Deri, G. Tevan, A. Semlyen, and A. Castanheira, "The Complex Ground Return Plane a Simplified Model for Homogeneous and Multi-Layer Earth Return," *IEEE Transactions on Power Apparatus and Systems*, vol. PAS-100, no. 8, pp. 3686–3693, 1981.

[42] T. Noda, "A Double Logarithmic Approximation of Carson's Ground-Return Impedance," *IEEE Transactions on Power Delivery*, vol. 21, no. 1, pp. 472–479, 2006.

[43] F. Rachidi, C. Nucci, and M. Ianoz, "Transient analysis of multiconductor lines above a lossy ground," *IEEE Transactions on Power Delivery*, vol. 14, no. 1, pp. 294–302, 1999.

[44] K. K. M. A. Kariyawasam, A. M. Gole, B. Kordi, and H. M. J. S. P. D. Silva, "Accurate Electromagnetic Transient Modelling of Sector-Shaped Cables," *International Conference on Power Systems Transients (IPST)*, 2011.

[45] S. a. Schelkunoff, "The Electromagnetic Theory of Coaxial Transmission Lines and Cylindrical Shields," *Bell System Technical Journal*, vol. 13, no. 4, pp. 532–579, 1934.

[46] L. Wedepohl and D. Wilcox, "Transient analysis of underground power-transmission systems. System-model and wave-propagation characteristics," *Proceedings of the Institution of Electrical Engineers*, vol. 120, no. 2, p. 253, 1973.

[47] P. de Arizon and H. W. Dommel, "Computation of Cable Impedances Based on Subdivision of Conductors," *IEEE Transactions on Power Delivery*, vol. 2, no. 1, pp. 21–27, 1987.

[48] L. J. Segerlind, *Applied Finite Element Analysis*, 2nd ed. New York: Wiley, 1984.

[49] L. Rubin, "Efficient conformal mapping technique for general transmission line parameter extraction," *IEEE Transactions on Magnetics*, vol. 29, no. 2, pp. 1380–1384, 1993.

[50] A. Timotin, "Uniqueness of solutions and power computation in the quasi-stationary electromagnetic field of parallel conductor system," *Revue roumaine des sciences techniques: Série électrotechnique et énergétique*, vol. 12, no. 3-4, 1967.

[51] T. R. Chandrupatla and A. D. Belegundu, *Introduction to Finite Elements in Engineering*, 4th ed. Prentice Hall, 2011.

[52] http://www.comsol.com.

[53] P. J. Olver, *Introduction to Partial Differential Equations*, 1st ed., ser. Undergraduate Texts in Mathematics. Cham: Springer International Publishing, 2014.

[54] E. Kreyszig, *Advanced Engineering Mathematics*, 9th ed. John Wiley & Sons, Inc., 2006.

[55] B. Kordi, G. E. Bridges, J. LoVetri, and J. E. Nordstrom, "Full-wave-based transmission-line model for lossy-substrate multiconductor interconnects," *International Journal of Numerical Modelling: Electronic Networks, Devices and Fields*, vol. 21, no. 1-2, pp. 103–115, 2008.

[56] S. Habib and B. Kordi, "Calculation of Multiconductor Underground Cables High-Frequency Per-Unit-Length Parameters Using Electromagnetic Modal Analysis," *IEEE Transactions on Power Delivery*, vol. 28, no. 1, pp. 276–284, 2013.

[57] R. Rivas and J. Marti, "Calculation of frequency-dependent parameters of power cables: matrix partitioning techniques," *IEEE Transactions on Power Delivery*, vol. 17, no. 4, pp. 1085–1092, 2002.

Appendix A

Cauchy-Riemann and the Mapping Factor

The Cauchy-Riemann condition in complex analysis is given by:

$$\frac{\partial u(x,y)}{\partial x} = \frac{\partial v(x,y)}{\partial y} \tag{A.1a}$$

$$\frac{\partial u(x,y)}{\partial y} = -\frac{\partial v(x,y)}{\partial x} \tag{A.1b}$$

The mapping factor (M) is defined by a combination of Equation A.1a and Equation A.1b:

$$M^2 \triangleq \left(\frac{\partial u}{\partial x}\right)^2 + \left(\frac{\partial u}{\partial y}\right)^2 = \left(\frac{\partial v}{\partial x}\right)^2 + \left(\frac{\partial v}{\partial y}\right)^2 \tag{A.2}$$

Combining Equation A.1a and Equation A.1b yields to:

$$\frac{\partial u}{\partial x}\frac{\partial v}{\partial x} + \frac{\partial u}{\partial y}\frac{\partial v}{\partial y} = -\frac{\partial u}{\partial x}\frac{\partial u}{\partial y} - \frac{\partial v}{\partial x}\frac{\partial v}{\partial y} = 0 \tag{A.3a}$$

$$\frac{\partial^2 u}{\partial x^2} = \frac{\partial}{\partial x}\left(\frac{\partial v}{\partial y}\right) = \frac{\partial}{\partial y}\left(\frac{\partial v}{\partial x}\right) = -\frac{\partial^2 u}{\partial y^2} \tag{A.3b}$$

$$\frac{\partial^2 v}{\partial x^2} = \frac{\partial}{\partial x}\left(-\frac{\partial u}{\partial y}\right) = \frac{\partial}{\partial y}\left(-\frac{\partial u}{\partial x}\right) = -\frac{\partial^2 v}{\partial y^2} \tag{A.3c}$$

$$\frac{\partial^2 u}{\partial x^2} + \frac{\partial^2 u}{\partial y^2} = \frac{\partial^2 v}{\partial x^2} + \frac{\partial^2 v}{\partial y^2} = 0 \tag{A.3d}$$

As mentioned in Section 3.1, there are two parameters that need to be determined in order to solve the problem: the electric scalar potential (V), and the z component of the magnetic vector potential (A_z). For the following derivations, V and A_z will be represented by Φ. Recalling that both parameters remain the same in the transformed space and that u and v are both functions of

x and y:

$$\Phi^T(u,v) = \Phi(x,y) \tag{A.4}$$

Applying Equation 3.7 to Φ:

$$\nabla^2\Phi = \frac{\partial^2\Phi}{\partial x^2} + \frac{\partial^2\Phi}{\partial y^2} \tag{A.5}$$

According to [49], it is necessary to determine the first and second partial derivatives of Φ in the transformed space, which is possible by using chain rule. The first partial derivatives are given by:

$$\frac{\partial\Phi}{\partial x} = \frac{\partial\Phi^T}{\partial u}\frac{\partial u}{\partial x} + \frac{\partial\Phi^T}{\partial v}\frac{\partial v}{\partial x} \tag{A.6a}$$

$$\frac{\partial\Phi}{\partial y} = \frac{\partial\Phi^T}{\partial u}\frac{\partial u}{\partial y} + \frac{\partial\Phi^T}{\partial v}\frac{\partial v}{\partial y} \tag{A.6b}$$

And the second partial derivatives can be determined by:

$$\begin{aligned}\frac{\partial^2\Phi}{\partial x^2} = {} & \frac{\partial^2\Phi^T}{\partial u^2}\left(\frac{\partial u}{\partial x}\right)^2 + \frac{\partial\Phi^T}{\partial u}\frac{\partial^2 u}{\partial x^2} + 2\frac{\partial}{\partial v}\left(\frac{\partial\Phi^T}{\partial u}\right)\frac{\partial u}{\partial x}\frac{\partial v}{\partial x} \\ & + \frac{\partial^2\Phi^T}{\partial v^2}\left(\frac{\partial v}{\partial x}\right)^2 + \frac{\partial\Phi^T}{\partial v}\frac{\partial^2 v}{\partial x^2}\end{aligned} \tag{A.7a}$$

$$\begin{aligned}\frac{\partial^2\Phi}{\partial y^2} = {} & \frac{\partial^2\Phi^T}{\partial u^2}\left(\frac{\partial u}{\partial y}\right)^2 + \frac{\partial\Phi^T}{\partial u}\frac{\partial^2 u}{\partial y^2} + 2\frac{\partial}{\partial v}\left(\frac{\partial\Phi^T}{\partial u}\right)\frac{\partial u}{\partial y}\frac{\partial v}{\partial y} \\ & + \frac{\partial^2\Phi^T}{\partial v^2}\left(\frac{\partial v}{\partial y}\right)^2 + \frac{\partial\Phi^T}{\partial v}\frac{\partial^2 v}{\partial y^2}\end{aligned} \tag{A.7b}$$

Substituting Equation A.7a and Equation A.7b in Equation A.5 yields to:

$$\begin{aligned}\nabla^2\Phi = {} & \frac{\partial^2\Phi^T}{\partial u^2}\left[\left(\frac{\partial u}{\partial x}\right)^2 + \left(\frac{\partial u}{\partial y}\right)^2\right] + \frac{\partial\Phi^T}{\partial u}\left(\frac{\partial^2 u}{\partial x^2} + \frac{\partial^2 u}{\partial y^2}\right) \\ & + \frac{\partial^2\Phi^T}{\partial v^2}\left[\left(\frac{\partial v}{\partial x}\right)^2 + \left(\frac{\partial v}{\partial y}\right)^2\right] + \frac{\partial\Phi^T}{\partial v}\left(\frac{\partial^2 v}{\partial x^2} + \frac{\partial^2 v}{\partial y^2}\right) \\ & + 2\frac{\partial}{\partial v}\left(\frac{\partial\Phi^T}{\partial u}\right)\left(\frac{\partial u}{\partial x}\frac{\partial v}{\partial x} + \frac{\partial u}{\partial y}\frac{\partial v}{\partial y}\right)\end{aligned} \tag{A.8}$$

Equation A.8 can be simplified by using Equation A.2, Equation A.3a and Equation A.3d yielding to:

$$\nabla^2\Phi = M^2\left(\frac{\partial^2\Phi}{\partial u^2} + \frac{\partial^2\Phi}{\partial v^2}\right) = M^2\left(\nabla^2\Phi^T\right) \tag{A.9}$$

The dot product between the gradient of two functions can be accomplished considering the two-dimensional quasi-electric assumption (the electric current flows only in the x-y plane). For

this purpose, let k be a complex function representing the electric or magnetic properties.

$$\begin{aligned}\nabla k \cdot \nabla \Phi &= \left(\frac{\partial k}{\partial x}\hat{\mathbf{a}}_x + \frac{\partial k}{\partial y}\hat{\mathbf{a}}_y\right) \cdot \left(\frac{\partial \Phi}{\partial x}\hat{\mathbf{a}}_x + \frac{\partial \Phi}{\partial y}\hat{\mathbf{a}}_y\right) \\ &= \frac{\partial k}{\partial x}\frac{\partial \Phi}{\partial x} + \frac{\partial k}{\partial y}\frac{\partial \Phi}{\partial y}\end{aligned} \tag{A.10}$$

Applying chain rule to Equation A.10 results in:

$$\nabla k \cdot \nabla \Phi = \left(\frac{\partial k^T}{\partial u}\frac{\partial u}{\partial x} + \frac{\partial k^T}{\partial v}\frac{\partial v}{\partial x}\right)\left(\frac{\partial \Phi^T}{\partial u}\frac{\partial u}{\partial x} + \frac{\partial \Phi^T}{\partial v}\frac{\partial v}{\partial x}\right) \tag{A.11}$$

where $k^T(u, v) = k(x, y)$

Rearranging terms in Equation A.11 yields to:

$$\begin{aligned}\nabla k \cdot \nabla \Phi = &\frac{\partial k^T}{\partial u}\frac{\partial \Phi^T}{\partial u}\left[\left(\frac{\partial u}{\partial x}\right)^2 + \left(\frac{\partial u}{\partial y}\right)^2\right] + \frac{\partial k^T}{\partial v}\frac{\partial \Phi^T}{\partial v}\left[\left(\frac{\partial v}{\partial x}\right)^2 + \left(\frac{\partial v}{\partial y}\right)^2\right] \\ &+ \frac{\partial k^T}{\partial u}\frac{\partial \Phi^T}{\partial v}\left(\frac{\partial u}{\partial x}\frac{\partial v}{\partial x} + \frac{\partial u}{\partial y}\frac{\partial v}{\partial y}\right) + \frac{\partial k^T}{\partial v}\frac{\partial \Phi^T}{\partial u}\left(\frac{\partial u}{\partial x}\frac{\partial v}{\partial x} + \frac{\partial u}{\partial y}\frac{\partial v}{\partial y}\right)\end{aligned} \tag{A.12}$$

From Equation A.2 and Equation A.3a, Equation A.12 simplifies to:

$$\nabla k \cdot \nabla \Phi = M^2\left(\frac{\partial k^T}{\partial u}\frac{\partial \Phi^T}{\partial u} + \frac{\partial k^T}{\partial v}\frac{\partial \Phi^T}{\partial v}\right) = M^2\left(\nabla k^T \cdot \nabla \Phi^T\right) \tag{A.13}$$

Appendix B

Bilinear Transformation Maps a Circle into a Circle

It is possible to prove that a circle in the real domain will remain a circle in the mapped space under a bilinear transformation by showing that applying the mapping scheme in the equation of a given circle in the mapped space:

$$(u - u_c)^2 + (v - v_c)^2 = R^2 \tag{B.1}$$

results in the equation of a circle in the real domain:

$$(x - x_c)^2 + (y - y_c)^2 = r^2 \tag{B.2}$$

where (u_c, v_c) and (x_c, y_c) are the centres of the circles with radii R and r in the mapped space and in the real domain, respectively.

Now, applying Equation 3.16 in Equation B.1 results in:

$$\left[\frac{2x}{x^2 + (1+y)^2} - \frac{2x_c}{x_c^2 + (1+y_c)^2}\right]^2 + \left[\frac{2(x^2 + y + y^2)}{x^2 + (1+y)^2} - \frac{2(x_c^2 + y_c + y_c^2)}{x_c^2 + (1+y_c)^2}\right]^2 = R^2 \tag{B.3}$$

which can be rearranged as:

$$(x - x_c)^2 + (y - y_c)^2 = \frac{1}{4}\left[x^2 + (1+y)^2\right]\left[x_c^2 + (1+y_c)^2\right] R^2 \tag{B.4}$$

From Equation B.4 it is possible to extract the relation between the mapped and real spaces radii as follows:

$$\frac{r^2}{R^2} = \frac{1}{4}\left[x^2 + (1+y)^2\right]\left[x_c^2 + (1+y_c)^2\right] \tag{B.5}$$